Journal of Human Genetics (2010) 55, 252–254

www.nature.com/jhg

SHORT COMMUNICATION

FALS with *FUS* mutation in Japan, with early onset, rapid progress and basophilic inclusion

Naoki Suzuki[1], Masashi Aoki[1], Hitoshi Warita[1], Masaaki Kato[1], Hideki Mizuno[1], Naoko Shimakura[1], Tetsuya Akiyama[1], Hirokazu Furuya[2], Toshihiro Hokonohara[3,4], Akiko Iwaki[3], Shinji Togashi[5], Hidehiko Konno[6] and Yasuto Itoyama[1]

Mutations in the *fused in sarcoma* (*FUS*, also known as *translated in liposarcoma*) gene have been recently discovered to be associated with familial amyotrophic lateral sclerosis (FALS) in African, European and American populations. In a Japanese family with FALS, we found the R521C *FUS* mutation, which has been reported to be found in various ethnic backgrounds. The family history revealed 23 patients with FALS among 46 family members, suggesting a 100% penetrance rate. They developed muscle weakness at an average age of 35.3 years, followed by dysarthria, dysphagia, spasticity and muscle atrophy. The average age of death was 37.2 years. Neuropathological examination of the index case revealed remarkable atrophy of the brainstem tegmentum characterized by cytoplasmic basophilic inclusion bodies in the neurons of the brainstem. We screened 40 FALS families in Japan and found 4 mutations (S513P, K510E, R514S, H517P) in exon 14 and 15 of *FUS*. Even in Asian races, FALS with *FUS* mutations may have the common characteristics of early onset, rapid progress and high penetrance rate, although in patients with the S513P mutation it was late-onset. Degeneration in multiple systems and cytoplasmic basophilic inclusion bodies were found in the autopsied cases.
Journal of Human Genetics (2010) **55,** 252–254; doi:10.1038/jhg.2010.16; published online 12 March 2010

Keywords: amyotrophic lateral sclerosis (ALS); basophilic inclusion; fused in sarcoma (FUS)

Amyotrophic lateral sclerosis is an adult-onset neurodegenerative disorder characterized by the death of motor neurons.[1] Approximately 20% of familial amyotrophic lateral sclerosis (FALS) cases are caused by mutations in the *superoxide dismutase 1* gene.[1,2] Mutations in the *TARDBP* gene, which codes for TAR DNA-binding protein 43 (TDP-43), have been recently reported in FALS cases.[3] Very recently, two groups of investigators reported the autosomal dominant form of FALS caused by *fused in sarcoma* (*FUS*) mutations,[4,5] following several reports of both familial and sporadic cases from Europe.[6–9] *FUS* is a nucleoprotein that functions in DNA and RNA metabolism.[10] In this study, we found a large Japanese FALS family with mutations in the *FUS* gene with the characteristics of early onset. In addition, we report four mutations of the *FUS* gene in Japanese FALS.

CASE REPORT OF THE INDEX CASE

The patient (indicated by arrow in Figure 1a) was a Japanese man with autosomal dominant hereditary burden as described in a previous report.[11] His family history revealed 23 patients with FALS over four generations (Figure 1a). He developed muscle weakness of the distal part of the right upper extremity at age 30, followed by dysarthria, dysphagia, muscle weakness and atrophy in the four extremities, spasticity, hyperreflexia and Babinski's sign. His sensory, cerebellar and higher cortical functions were not affected. At age 31 (17 months after onset) he needed ventilatory support. At age 40, he died of bronchopneumonia.

MATERIALS AND METHODS

All patients of FALS without the *superoxide dismutase 1* mutation and healthy controls provided informed consent, after which DNA extraction and genotyping were performed using standard protocols as described elsewhere.[12] We sequenced all exons in 40 unrelated FALS families with the characteristics of an autosomal dominant trait in Japan. Sections of 5 μm thickness were taken from the midbrain of the index case and stained as described elsewhere.[5] Rabbit polyclonal anti-TDP-43 (ProteinTech, Chicago, IL, USA) and rabbit polyclonal anti-ubiquitin (Abcam, Cambridge, MA, USA) antibodies were used. The study was approved by the ethics committee and all subjects gave written informed consent.

RESULTS

We detected a missense mutation (C1561T) in the *FUS* gene that substituted cysteine for arginine at residue 521 (R521C) (Figure 1c) in the index case. Family history revealed 23 patients with FALS among

[1]Department of Neurology, Tohoku University School of Medicine, Sendai, Japan; [2]Department of Neurology, Neuro-Muscular Center, National Oomuta Hospital, Fukuoka, Japan; [3]Division of Human Molecular Genetics, Research Center for Genetic Information, Medical Institute of Bioregulation, Kyushu University, Fukuoka, Japan; [4]Department of Neurology, Neurological Institute Graduate School of Medical Sciences, Kyushu University, Fukuoka, Japan; [5]Department of Neurology, Kofu City Hospital, Kofu, Japan and [6]Department of Neurology, Nishitaga National Hospital, Sendai, Japan
Correspondence: Dr M Aoki, Department of Neurology, Tohoku University School of Medicine, 1-1 Seiryo-machi, Sendai 980-8574, Japan.
E-mail: aokim@mail.tains.tohoku.ac.jp
Received 8 November 2009; revised 2 February 2010; accepted 8 February 2010; published online 12 March 2010

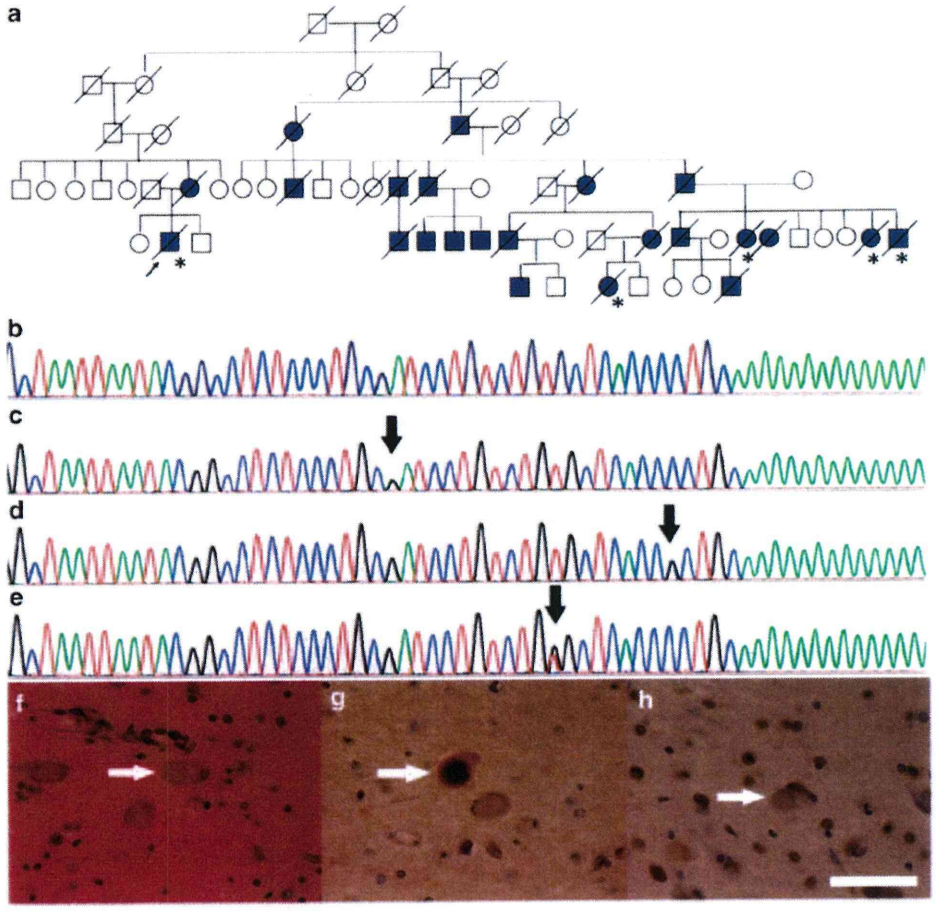

Figure 1 (**a**) Pedigree of a Japanese family with FALS with *FUS* mutations. Males are represented by squares, females by circles. Affected members are represented by solid symbols, deceased individuals by diagonals. The proband is indicated by an arrow. Autopsied cases are marked with asterisks. (**b**–**e**) Sequence electropherogram of the *FUS* gene. (**b**) Sequence of a normal subject; (**c**) sequence of the index case with a missense mutation (C1561T) in exon 15 of the *FUS* gene that substituted cysteine for arginine at residue 521 (R521C); (**d**) arginine for serine at residue 514 (R514S); and (**e**) sequence of the other case with histidine for proline at residue 517 (H517P). The arrows indicate the substitution site. (**f**–**h**) Hematoxylin–eosin staining and immunohistochemistry of the midbrain from the index case. A few basophilic inclusion bodies were present in the neurons of the brain stem (**f**, arrow). These basophilic bodies were stained with ubiquitin (**g**, arrow), but not with TDP43 (**h**, arrow). Scale bar, 50 μm.

46 family members, suggesting a 100% penetrance rate. The average age at disease onset was 35.3 ± 5.1 years (n=12). The disease duration (from onset to respiratory failure) of the cases with the R521C mutation was 16.1 ± 7.7 months. The disease course was rapidly progressive and the average age at death was 37.2 ± 4.2 years (n=12). We found no case with cognitive impairment among the FALS patients with FUS mutations.

Neuropathological examination of the case (indicated by the arrow in Figure 1a) revealed not only neuronal loss in the upper and lower motor neuron systems and Clarke's column, but also degeneration of the pyramidal tracts, middle root zone of the posterior column and the posterior spinocerebellar tract. Atrophy of the brainstem tegmentum was remarkable. Neuronal loss and astrocytosis in the globus pallidus, substantia nigra, locus ceruleus and subthalamic nucleus were associated with eosinophilic granular bodies. A few basophilic inclusion bodies were exclusively present in the neurons of the brainstem (indicated by the arrow in Figure 1f) as previously reported.[11] These basophilic bodies were immunohistochemically stained with ubiquitin (Figure 1g), not with TDP-43 (Figure 1h).

We also found four mutations, serine for proline at residue 513 (S513P), arginine for serine at residue 514 (R514S; Figure 1d), lysine for glutamate at residue 510 (K510E) in exon 14 and histidine for proline at residue 517 (H517P; Figure 1e) in exon 15 of *FUS*. These patients showed the characteristics of early onset at around age 30, and rapid progress, although the age at onset in patients with the S513P mutation was around 60. S513P, R514S and H517P are novel mutations. The lower motor neurons were mainly affected in these patients with *FUS* mutations. The case with the S513P mutation progressed slowly and was followed up as a case of spinal progressive muscular atrophy with family history. Exos 14 and 15 of the *FUS* gene were sequenced in 100 Japanese healthy controls and no mutations were detected.

DISCUSSION

Mutations in the *FUS* gene have been reported to be associated with FALS in African, European and American populations.[4–9] We found the *FUS* mutation in a Japanese family with FALS with the characteristics of early onset, rapid progress, high penetrance, degeneration of

the multiple system, remarkable atrophy of the brainstem tegmentum and basophilic inclusion bodies in the autopsy. The immunohistochemical findings of the basophilic inclusion bodies of our case were recognized by using ubiquitin, but not by using antibodies to tau, neurofilament[11] or TDP-43. Very recently, an FUS abnormality was found in basophilic inclusion body disease including motor neuron disease.[13,14] Although the role of basophilic inclusion remains to be elucidated, this study underscores the importance of basophilic inclusion and FUS in the pathological process of amyotrophic lateral sclerosis. The basophilic inclusions were exclusively found in the brainstem tegmentum in our cases, although the number was small and the distribution of basophilic inclusion bodies may depend on the timing of autopsy. By using an animal model with mutations in exon 15 of *FUS*, it may be feasible to study the relationship between the disease course and basophilic inclusion.

The phenotype–genotype correlation in amyotrophic lateral sclerosis with *FUS* mutations is not well established.[15] Vance *et al.*[4] reported that the average age at onset was 44.5 years and average survival was 33 months in FALS with *FUS* gene mutations. Even in Asian races, FALS with *FUS* mutations may have the common characteristics of early onset and rapid progression, especially in patients with the R521C mutation, which is found in patients of various ethnic backgrounds. On the other hand, patients with the S513P mutation had late-onset disease. It is not clear why differences in the phenotypes among these mutations occurred, although all mutations were concentrated in the extreme C-terminus of the *FUS* gene. The accumulation of clinical, genetic and pathological information will be necessary to elucidate the pathomechanism of motor neuron death in FALS with *FUS* mutations.

CONFLICT OF INTEREST

The authors declare no conflict of interest.

ACKNOWLEDGEMENTS

This work was supported by Research Grants from Nervous and Mental disorders (20B-13), Research on Measures for Intractable Diseases, Research on Psychiatric and Neurological Diseases and Mental Health from the Japanese Ministry of Health Labor and Welfare, Grants-in-Aids for Scientific Research (21591070) and Grants-in-Aids for Young Scientist (19890016) from the Japanese Ministry of Education, Culture, Sports, Science and Technology.

1 Pasinelli, P. & Brown, R. H. Molecular biology of amyotrophic lateral sclerosis: insights from genetics. *Nat. Rev. Neurosci.* **7,** 710–723 (2006).
2 Rosen, D. R., Siddique, T., Patterson, D., Figlewicz, D. A., Sapp, P., Hentati, A. *et al.* Mutations in Cu/Zn superoxide dismutase gene are associated with familial amyotrophic lateral sclerosis. *Nature* **362,** 59–62 (1993).
3 Kabashi, E., Valdmanis, P. N., Dion, P., Spiegelman, D., McConkey, B. J., Vande Velde, C *et al.* TARDBP mutations in individuals with sporadic and familial amyotrophic lateral sclerosis. *Nat. Genet.* **40,** 572–574 (2008).
4 Vance, C., Rogelj, B., Hortobágyi, T., De Vos, K. J., Nishimura, A. L., Sreedharan, J. *et al.* Mutations in FUS, an RNA processing protein, cause familial amyotrophic lateral sclerosis type 6. *Science* **323,** 1208–1211 (2009).
5 Kwiatkowski, T. J. Jr, Bosco, D. A., Leclerc, A. L., Tamrazian, E., Vanderburg, C. R., Russ, C. *et al.* Mutations in the FUS/TLS gene on chromosome 16 cause familial amyotrophic lateral sclerosis. *Science* **323,** 1205–1208 (2009).
6 Talbot, K. Another gene for ALS: mutations in sporadic cases and the rare variant hypothesis. *Neurology* **73,** 1172–1173 (2009).
7 Belzil, V. V., Valdmanis, P. N., Dion, P. A., Daoud, H., Kabashi, E., Noreau, A. *et al.* Mutations in FUS cause FALS and SALS in French and French Canadian populations. *Neurology* **73,** 1176–1179 (2009).
8 Chio, A., Restagno, G., Brunetti, M., Ossola, I., Calvo, A., Mora, G. *et al.* Two Italian kindreds with familial amyotrophic lateral sclerosis due to FUS mutation. *Neurobiol. Aging* **30,** 1272–1275 (2009).
9 Corrado, L., Del Bo, R., Castellotti, B., Ratti, A., Cereda, C., Penco, S. *et al.* Mutations of FUS gene in sporadic amyotrophic lateral sclerosis. *J. Med. Genet.* (e-pub ahead of print 26 October) (2009).
10 Wang, X., Arai, S., Song, X., Reichart, D., Du, K., Pascual, G. *et al.* Induced ncRNAs allosterically modify RNA-binding proteins in cis to inhibit transcription. *Nature* **454,** 126–130 (2008).
11 Tsuchiya, K., Matsunaga, T., Aoki, M., Haga, C., Ooe, K., Abe, K. *et al.* Familial amyotrophic lateral sclerosis with posterior column degeneration and basophilic inclusion bodies: a clinical, genetic and pathological study. *Clin. Neuropathol.* **20,** 53–59 (2001).
12 Aoki, M., Lin, C. L., Rothstein, J. D., Geller, B. A., Hosler, B. A., Munsat, T. L. *et al.* Mutations in the glutamate transporter EAAT2 gene do not cause abnormal EAAT2 transcripts in amyotrophic lateral sclerosis. *Ann. Neurol.* **43,** 645–653 (1998).
13 Munoz, D. G., Neumann, M., Kusaka, H., Yokota, O., Ishihara, K., Terada, S. *et al.* FUS pathology in basophilic inclusion body disease. *Acta Neuropathol.* **118,** 617–627 (2009).
14 Neumann, M., Rademakers, R., Roeber, S., Baker, M., Kretzschmar, H. A. & Mackenzie, I. R. A new subtype of frontotemporal lobar degeneration with FUS pathology. *Brain* **132,** 2922–2931 (2009).
15 Lagier-Tourenne, C. & Cleveland, D. W. Rethinking ALS: the FUS about TDP-43. *Cell* **136,** 1001–1004 (2009).

Journal of the Neurological Sciences 294 (2010) 95–101

Contents lists available at ScienceDirect

Journal of the Neurological Sciences

journal homepage: www.elsevier.com/locate/jns

Neuronal NOS is dislocated during muscle atrophy in amyotrophic lateral sclerosis

Naoki Suzuki [a,*], Hideki Mizuno [a], Hitoshi Warita [a], Shin'ichi Takeda [b], Yasuto Itoyama [a], Masashi Aoki [a]

[a] Department of Neurology, Tohoku University School of Medicine, 1-1 Seiryo-machi, Aoba-ku, Sendai 980-8574, Japan
[b] Department of Molecular Therapy, National Institute of Neuroscience, National Center of Neurology and Psychiatry, Kodaira, Tokyo 187-8502, Japan

ARTICLE INFO

Article history:
Received 1 September 2009
Received in revised form 23 March 2010
Accepted 23 March 2010

Keywords:
Amyotrophic lateral sclerosis (ALS)
Motor neuron disease (MND)
Muscle atrophy
Neuronal nitric oxide synthase (nNOS)
Superoxide dismutase (SOD1)

ABSTRACT

Previously, we demonstrated that neuronal nitric oxide synthase (nNOS) is activated and promotes muscle atrophy in skeletal muscle during tail suspension, a model of unloading and denervation. Here, we examined patients with amyotrophic lateral sclerosis (ALS) and mutant (H46R) SOD1 transgenic (Tg) mice model using immunohistochemistry, Western blotting and real time PCR. We found cytoplasmic nNOS staining of angulated muscle fibers in patients with ALS. We also examined mutant SOD1 Tg mice and found cytoplasmic nNOS staining even before the onset of clinical muscle atrophy. In the Tg mice, nNOS was largely extracted with 100 mM NaCl and barely detected in the pellet fraction, suggesting fragile anchoring of nNOS to the sarcolemma. We also showed an elevated expression of atrogin-1, key molecules in muscle atrophy at the end stage. A common nNOS dislocation/atrogin-1/muscle atrophy pathway among tail suspension, denervation and ALS is suggested. nNOS modulation therapy may be beneficial in several types of muscle atrophy.

1. Introduction

Amyotrophic lateral sclerosis (ALS) is a fatal neurodegenerative disease caused by the selective death of motor neurons [1–3]. Approximately 10% of the cases of ALS are inherited, usually as an autosomal dominant trait. In 25% of familial cases, the disease is caused by mutations in the gene encoding cytosolic copper–zinc superoxide dismutase (SOD1) [4–6]. The reason why the motor neuron is selectively damaged has not been elucidated. Additionally, the mechanism of muscle atrophy followed by motor neuron death has not been resolved. The overexpression of mutant human SOD1 in mice is used as a model of ALS. These mutant SOD1 transgenic (Tg) mice reproduce the major phenotypic features of human ALS [7,8], and could be used in analyzing the pathomechanism of ALS [9,10].

Reduced muscle activity such as bed rest, limb immobilization, denervation, or unloading (e.g. tail suspension or space flight) leads to significant muscle atrophy [11,12]. In these conditions, the atrophying muscles show increased rates of protein degradation mainly through the activation of the ubiquitin proteasome system [13,14], and the muscle-specific E3 ubiquitin ligases, Muscle-specific RING finger protein 1 (MuRF-1) and atrogin-1/Muscle atrophy F-box protein (MAFbx), are commonly up-regulated [13,14]. Recent studies further showed that muscle inactivity results in the suppression of the IGF-1/PI3k/Akt pathway [15–18] and activation of transcription factors such as the Foxo family and NFκB [19–21].

Several molecules are proposed as a mechanical sensor or a trigger of disuse atrophy. It has been reported that muscles from tumor-bearing mice exhibited reduced levels of dystrophin, the protein that is mutated in Duchenne muscular dystrophy, together with a reduction of dystrophin-associated glycoprotein [22,23]. These results raise the possibility that the dystrophin glycoprotein complex (DGC) works as a regulator of muscle atrophy or serves as a scaffold for anti-atrophic signal transduction.

Recently, we examined the expression and function of the members of DGC in skeletal muscle during tail suspension, a model of unloading, and demonstrated that neuronal nitric oxide synthase (nNOS), a member of DGC, is activated in unloading conditions and promotes muscle atrophy [24]. We also showed that a nNOS-specific inhibitor significantly attenuates suspension-induced muscle atrophy. Furthermore, we showed the involvement of nNOS in the denervation-induced muscle atrophy process. Thus, nNOS and nitric oxide (NO) are new therapeutic targets for disuse-induced muscle atrophy.

We hypothesized that the same phenomena exist under the pathomechanism of ALS. For the purpose of examining the pathomechanism of muscle atrophy in ALS, here we examined muscles from patients with ALS and a mouse model of ALS. We found nNOS dislocation during the disease process of mutant SOD1 Tg mice. A common nNOS dislocation/atrogin-1 pathway for tail suspension, denervation and ALS induced muscle atrophy is suggested.

Abbreviations: ALS, amyotrophic lateral sclerosis; DGC, dystrophin glycoprotein complex; eNOS, endothelial nitric oxide synthase; Gc, gastrocnemius; H46R, histidine to arginine at position 46; iNOS, inducible nitric oxide synthase; MAFbx, Muscle atrophy F-box protein; MuRF-1, Muscle-specific RING finger protein 1; nNOS, neuronal nitric oxide synthase; NO, nitric oxide; SOD1, superoxide dismutase 1; TA, tibialis anterior; Tg, transgenic.

* Corresponding author. Tel.: +81 22 717 7189; fax: +81 22 717 7192.
E-mail address: naoki@em.neurol.med.tohoku.ac.jp (N. Suzuki).

0022-510X/$ – see front matter © 2010 Elsevier B.V. All rights reserved.
doi:10.1016/j.jns.2010.03.022

Table 1
Patients list. Characteristics and immunostaining results of patients with ALS and normal control. ALS, amyotrophic lateral sclerosis; BB, biceps brachii; RF, rectus femoris; TA, tibialis anterior; M, male; F, female.

No.	Sex	Age	Disease	Months after onset	nNOS membrane	nNOS cytosol	α1-syntrophin	Site of biopsy
1	M	71	ALS	4	+	+	+	BB
2	F	58	ALS	7	+	−	+	BB
3	M	47	ALS	8	+	+	+	TB
4	F	55	ALS	8	+	+	+	BB
5	M	45	ALS	13	+	+	+	TA
6	M	67	ALS	20	+	−	+	RF
7	M	70	ALS	30	+	+	+	TA
8	F	68	ALS	48	+	−	+	TA
9	F	47	ALS	144	+	+	+	BB
10	M	46	ALS	300	+	+	+	BB
11	M	19	Normal	–	+	−	+	BB
12	F	59	Normal	–	+	−	+	BB
13	M	29	Normal	–	+	−	+	BB

2. Methods

2.1. Patients

We studied skeletal muscle biopsies obtained from 10 patients who had, according to the El Escorial criteria, a diagnosis of definite ALS at the Department of Neurology, Tohoku University School of Medicine. No patients had a family history of motor neuron disease. The patients were 6 males and 4 females, with the age at the time of muscle biopsy between 45 and 71 years, as shown in Table 1. At the time of biopsy, the duration of disease was 4–300 months. Muscle biopsy was performed with each patient's written informed consent. The routine histochemical analysis of all biopsies showed neurogenic changes ranging from mild to severe. We used 3 normal patients as positive controls and Becker type muscular dystrophy diagnostic muscle biopsies as negative controls for nNOS staining.

2.2. The clinical course of H46R SOD1 transgenic mice

Transgenic (Tg) mice expressing H46R mutant human SOD1 were generated as described previously [7,8,25–28]. The Tg mice developed motor neuron disease with a mean age of onset in clinical weakness of approximately 21 weeks. In each Tg mouse we carefully observed the development of the symptoms of ALS. Clinically apparent weakness,

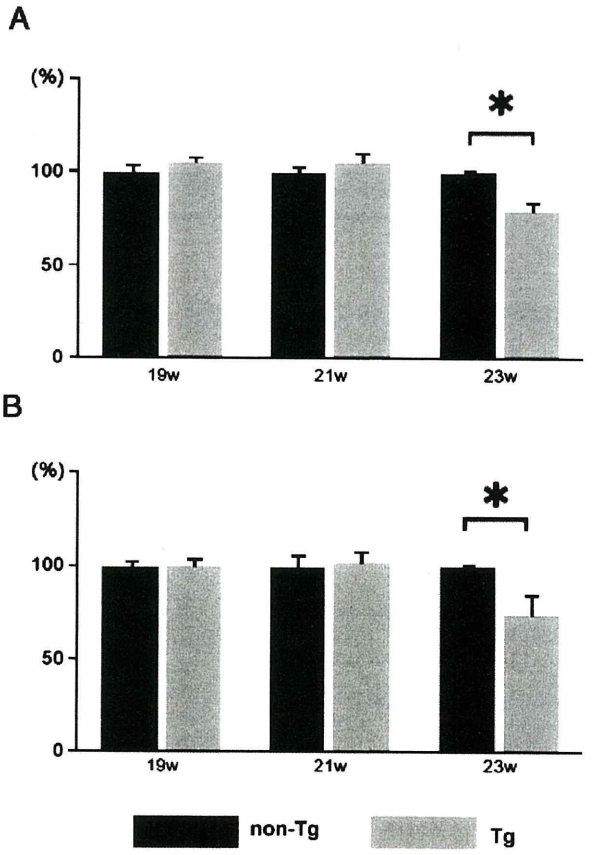

Fig. 2. Muscle weight during the disease course of mutant SOD1 Tg mice. Weights of TA (A) and Gc (B) muscles from Tg and non-Tg mice are normalized to body weight, and are expressed as percentage of non-Tg mice of each age ($n=5$ for each group). Student's t-test, $^*p<0.05$.

indicated by dragging of one hindlimb without limb tremor, was evident somewhat later. Simultaneously with the onset of clinical weakness, the affected mice showed prominent muscle atrophy and weight loss. While the initial clinical manifestation of weakness was unilateral leg paralysis, this progressed and became bilateral in the Tg mice. In the early stages of the illness, another distinctive abnormality

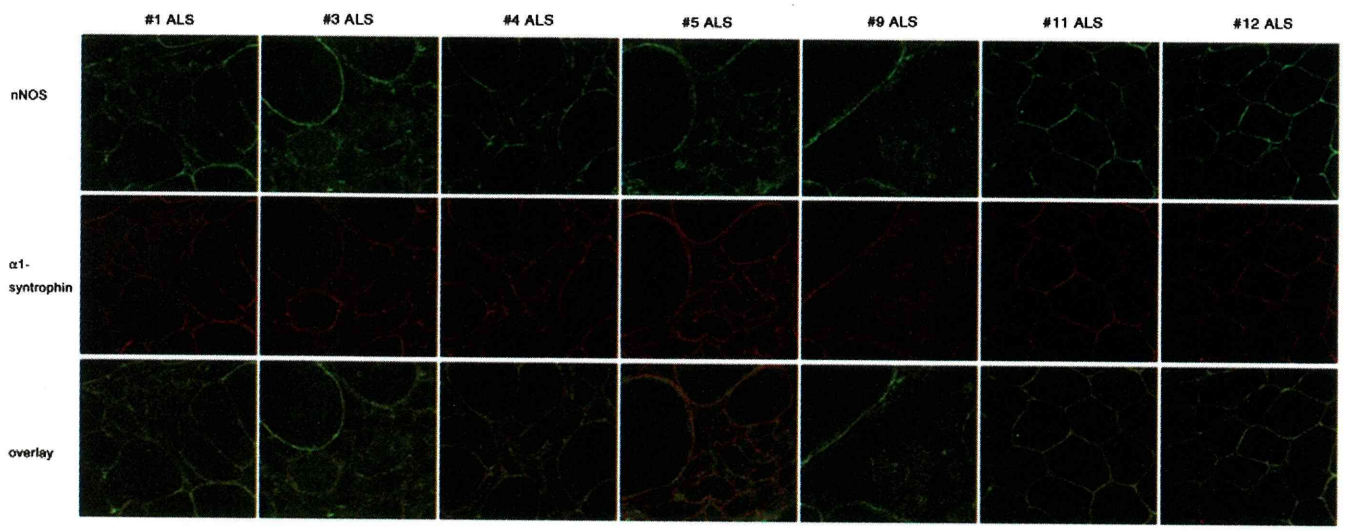

Fig. 1. Dislocation of nNOS is observed in patients with ALS. nNOS in normal and affected muscles was stained with nNOS and α1-syntrophin antibodies. Overlay image is also presented. Scale bar, 50 μm.

was the increased tone in the tail musculature, resulting in an elevated, segmentally spastic tail posture. At end stage, the affected mice could not drink water and died. The mean age at death from the disease was around 24 weeks. The animals were allowed ad libitum access to food and drinking water. The animals were sacrificed by cervical dislocation, and the tibialis anterior (TA) and gastrocnemius (Gc) muscles were excised for analysis. All experimental protocols and procedures were approved by the Animal Committee of the Tohoku University School of Medicine, Japan.

2.3. Tissue preparation from Tg mice

Body and wet muscle were weighed. The TA and Gc muscles were collected individually using standard dissection methods and cleaned of excess fat, connective tissue, and tendons. Several of the muscles were frozen in isopentane cooled by liquid nitrogen for histological and immunohistochemical analysis, and the other muscles were frozen directly in liquid nitrogen for RNA isolation or protein extraction and stored at −80 °C.

2.4. Real time PCR

Total RNA was isolated using TRIzol (Invitrogen, Carlsbad, CA). For real time PCR, first strand cDNA was synthesized using oligo-dT primers. The expression levels of selected genes (nNOS, MuRF-1, atrogin-1/MAFbx and β-actin) were analyzed using LightCycler (Roche, Basel, Switzerland) following the manufacturer's instructions.

2.5. Immunohistochemistry

Cryostat sections of muscle tissue (10 μm thick) cut in the middle part of the TA muscle belly to obtain the largest myofiber diameter, were placed on poly-L-lysine-coated slides, air dried, and, post-fixed in acetone at −20 °C and pre-incubated in phosphate-buffered saline (PBS) containing 5% goat serum and 1% bovine serum albumin for 30 min at room temperature. Polyclonal anti-nNOS (Invitrogen) and anti-α1-syntrophin (Biogenesis, Poole, UK) were applied overnight at 4 °C. Following incubations with the appropriate secondary antibodies, mounted sections were observed by using an Olympus confocal microscope (Tokyo, Japan). nNOS dislocated fibers per 100 muscle fibers were counted in mutant SOD1 Tg mice and control mice.

2.6. Western blotting

Total skeletal muscle protein was extracted from mouse Gc muscle for Western blot analysis. We used the Bradford method to determine the protein concentrations. Then, protein fractions were extracted with a reducing sample buffer containing 2.3% SDS, 70 mM Tris–HCl, 5% β-mercaptoethanol and Complete inhibitor cocktail (Roche). Protein (30 μg per lane) was separated on a 10–20% gradient SDS-polyacrylamide gel. The resulting gel was subsequently transferred to

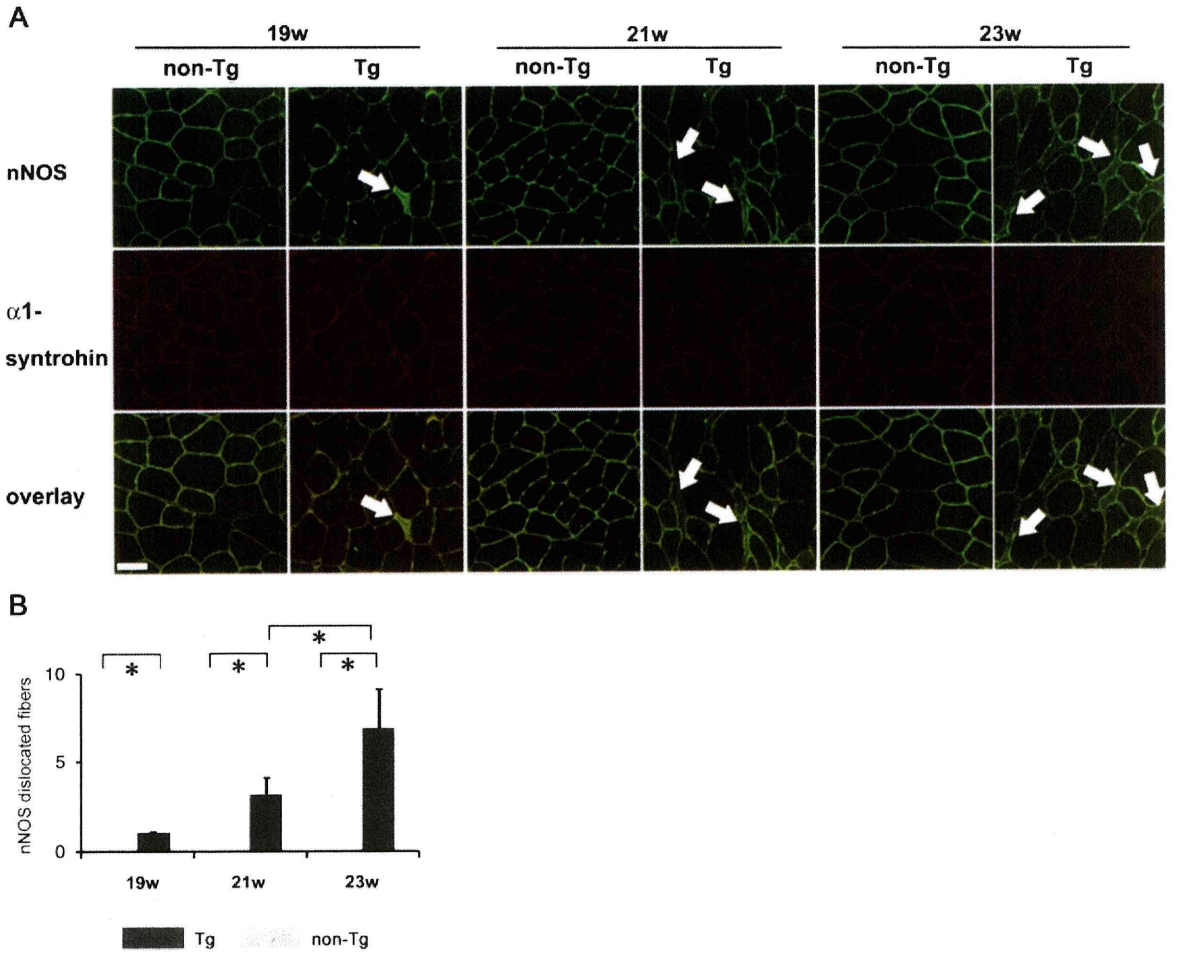

Fig. 3. Localization of nNOS during the disease course of mutant SOD1 Tg mice. (A) Transverse muscle sections from 19 weeks (w), 21 w, 23 w Tg and non-Tg mice were stained with anti-nNOS and α1-syntrophin antibodies. An overlay image is also presented. Scale bar, 50 μm. Arrows represent the nNOS dislocated angulated fibers. (B) nNOS dislocated fibers per 100 muscle fibers were counted in mutant SOD1 Tg mice and control mice. ($n = 5$ for each group). Student's t-test, $^*p < 0.05$.

a polyvinylidene difluoride membrane (Millipore, Billerica, MA) using 242 mA for 1 h. The blot was later incubated with primary antibodies. The signals were detected using the enhanced chemiluminescence method (GE Healthcare, Piscataway, NJ). The following antibodies were used for immunoblotting: anti-α1-syntrophin, anti-aquaporin-4 (Chemicon, Billerica, MA), anti-caveolin-3, α-sarcoglycan, β1-sarcoglycan, dystrobrevin (Novocastra, Newcastle upon Tyne, UK), anti-nNOS (BD Biosciences, Franklin Lakes, NJ), GAPDH, inducible NOS (iNOS) (Santa Cruz Biotechnology, Santa Cruz, CA), and endothelial NOS (eNOS) (Cayman Chemicals, Ann Arbor, MI) antibodies. The bands were quantified in densitometry using Image-J [24].

2.7. Subcellular fractionation

The subcellular fractionation was performed according to the method described by Brenman et al. [29] and described previously [24]. Briefly, the Gc muscle was homogenized in 10 volumes (w/v) of buffer A (25 mM Tris–HCl, pH 7.4, 100 mM NaCl, 1 mM EDTA, 1 mM EGTA). The nuclei of the muscle were pelleted by centrifugation at 1000×g. The supernatant was then centrifuged at 20,000×g to yield supernatant S1. The resulting heavy microsomal pellet was resuspended in buffer B (500 mM NaCl added to buffer A), incubated for 30 min at 4 °C with agitation, and centrifuged at 15,000×g, yielding supernatant S2. The pellet from this last centrifugation was resuspended in buffer B containing 0.5% Triton X-100, incubated for 30 min at 4 °C with agitation, and centrifuged at 15,000×g to create supernatant S3 and the final pellet, P. The fractions were resolved using the sample buffer and analyzed by SDS-polyacrylamide gel electrophoresis. The bands are quantified in densitometry.

2.8. Statistical analysis

Statistical differences were determined by either Student's unpaired *t*-test or the Mann–Whitney test. All data are expressed as means ± s.e.m. Statistical significance was defined as $p<0.05$ (asterisk).

3. Results

3.1. Dislocated nNOS is observed in human ALS patients

Previously, we demonstrated that neuronal nitric oxide synthase (nNOS) is activated and promotes muscle atrophy in skeletal muscle during tail suspension, a model of unloading and denervation. To examine whether nNOS is involved in the pathomechanism of ALS, we first stained biopsied human skeletal muscle samples of ALS patients with nNOS and α1-syntrophin (Table 1 and Fig. 1). These patients were all sporadic cases. In the muscle of control patients nNOS was localized only at the sarcolemma. The nNOS staining patterns were co-localized with α1-syntrophin. We found nNOS staining of the cytoplasm in some atrophied muscle fibers in ALS patients. Some nNOS dislocated fibers were abnormally small, round or hypertrophied muscle fibers. As a negative control of immunohistochemistry for nNOS, we used Becker type muscular dystrophy in which nNOS protein is not stained at the sarcolemma (data not shown). The nNOS dislocation would have no relation to the extent of muscle atrophy or disease duration in this small sample size due to the variation of the disease course in human ALS. These results prompted us to study the role of dislocated nNOS during the disease course of the mutant SOD1 Tg mice.

3.2. Dislocated nNOS is observed before the onset of muscle atrophy in Tg mice

To elucidate the molecular mechanisms of muscle atrophy in ALS, female H46R mutant SOD1 Tg mice [8,25] were divided into 3 groups (8 mice each): pre-symptomatic (aged 19 weeks), onset (aged 21 weeks, just after onset) and end stage (aged 23 weeks); and examined with age-matched non-Tg littermate controls. The weight of the TA and Gc muscles/body weight was decreased to ~80% of the control mice at the end stage in this mice model (Fig. 2).

The immunohistochemical expression patterns of the components of DGC, dystrophin, laminin-α2, α1-syntrophin, and caveolin-3 were not changed during the disease course (Fig. 3 and data not shown). Importantly, immunohistochemistry revealed that nNOS was dislocated from the sarcolemma to the cytoplasm even before and at the onset of disease (Fig. 3). We also found increasing numbers of nNOS dislocated fibers as the disease progressed. The nNOS mRNA levels were not significantly reduced (data not shown), and total nNOS protein was not changed (Fig. 4A). Subcellular fractionation revealed a faint amount of nNOS in the P (pellet) fraction at the disease onset (Fig. 4B,C). Otherwise, S1 (soluble) fraction revealed no change in nNOS and α1-syntrophin. iNOS, another member of the NOS family, was significantly increased in the Tg mice (Fig. 5A,C). eNOS and other members of DGC (caveolin-3, α1-syntrophin, aquaporin-4, α, β-sarcoglycan and dystrobrevin) were not changed during the disease course (Fig. 5A–C). These results indicate that nNOS dislocates to the cytoplasm and iNOS is abnormally expressed during the disease course.

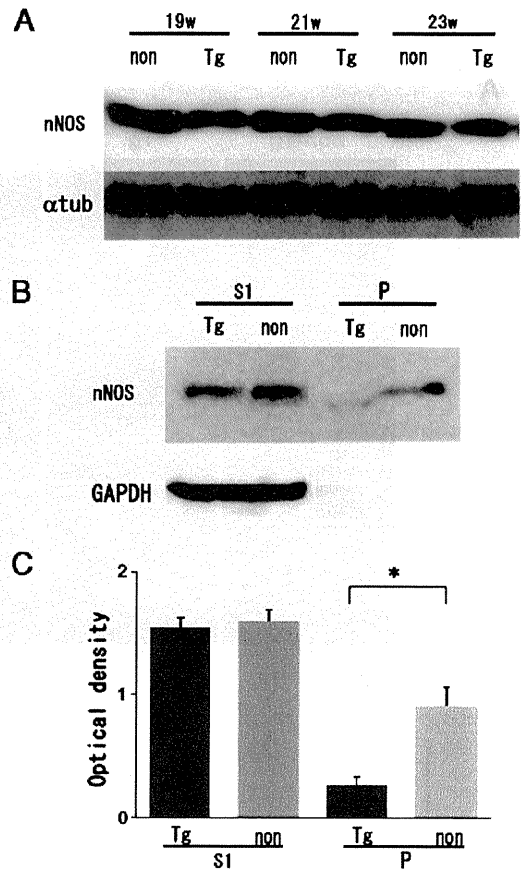

Fig. 4. Western blotting and subcellular fractionation of nNOS in mutant SOD1 Tg mice. (A) Immunoblots of mouse Gc muscle extracts for nNOS from 19 weeks (w), 21 w, 23 w Tg and non-Tg mice. All lanes contain 30 μg of total protein. The experiments were performed 3 times and representative pictures are presented. (B) Subcellular fractionation of Gc muscle extracts from 21 w Tg and non-Tg mice staining for nNOS and GAPDH. P indicates insoluble pellet after sequential extraction of skeletal muscle homogenates with 100 mM NaCl (S1), 500 mM NaCl, and 0.5% Triton X-100. Representative data are presented. (C) Quantification of nNOS signals in S1 and P fractions of muscle extracts shown in B ($n=4$/each group). Mann–Whitney test, $^*p<0.05$.

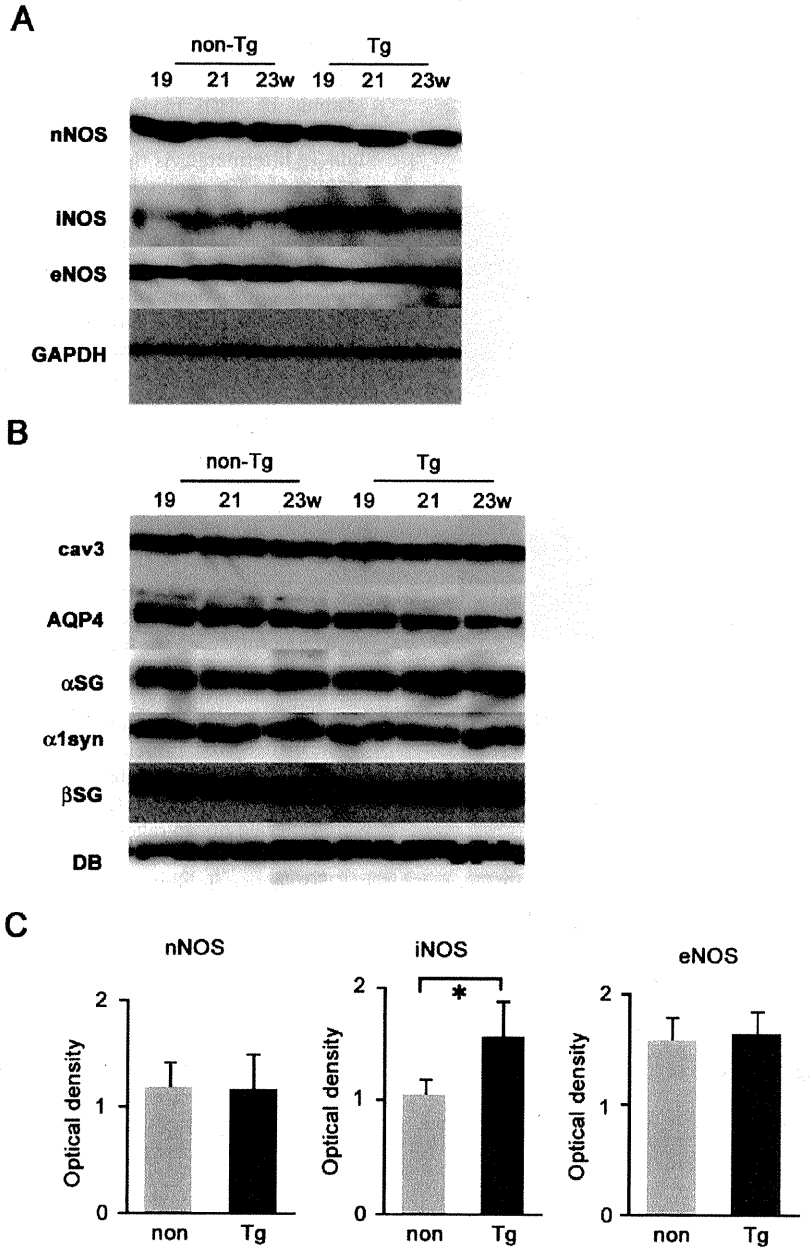

Fig. 5. Total amounts of proteins of NOS family and DGC components during the disease course in mutant SOD1 Tg mice. (A) Immunoblots of mouse Gc muscle extracts for NOS family and GAPDH from 19 weeks (w), 21 w, 23 w Tg and non-Tg mice. (B) Immunoblots of mouse Gc muscle extracts for DGC components from 21-week-old Tg and non-Tg mice. All lanes contain 30 μg of total protein. The experiments were performed 3 times and representative pictures are presented. αsyn, α1-syntrophin; AQP4, aquaporin-4; cav3, caveolin-3; αSG, α-sarcoglycan; βSG, β1-sarcoglycan; DB, dystrobrevin. (C) The amounts of nNOS, iNOS, and eNOS in Tg and non-Tg mice were quantified ($n = 4$). Mann–Whitney test, $^*p<0.05$.

Previously, we reported that the dislocated nNOS produces excessive NO and ends in muscle atrophy during tail suspension [24]. Recently, several groups have pointed out that the ubiquitin proteasome pathway is largely involved in selective protein degradation during the muscle atrophy process [13,14,30]. In our previous study [24], we found no elevation of E3 ubiquitin ligases during tail suspension in nNOS-null muscle, although we found the elevation of E3 ubiquitin ligases in wild type muscle, suggesting up-regulations of E3 ubiquitin ligases were downstream events of nNOS dislocation in muscle atrophy. Consistent with this, the mRNA levels of the muscle-specific E3 ubiquitin ligase, atrogin-1/MAFbx (not MuRF1), were significantly increased in the mutant SOD1 Tg mice at the end stage (Fig. 6A,B).

4. Discussion

In our previous report, we demonstrated for the first time that nNOS is dislocated from the sarcolemma to the cytoplasm during tail suspension and denervation, whereas other members of DGC are normally expressed at the sarcolemma [24]. Here we demonstrated the dislocation of nNOS during the disease course of human ALS and a mouse model of ALS. The time point of nNOS dislocation was around the onset of the disease but before the apparent progression of muscle atrophy.

NO possesses both neuroprotective and neurodegenerative effects in the nervous system [31,32]. There are several reports on the relationship between ALS and nNOS, focusing especially on the spinal

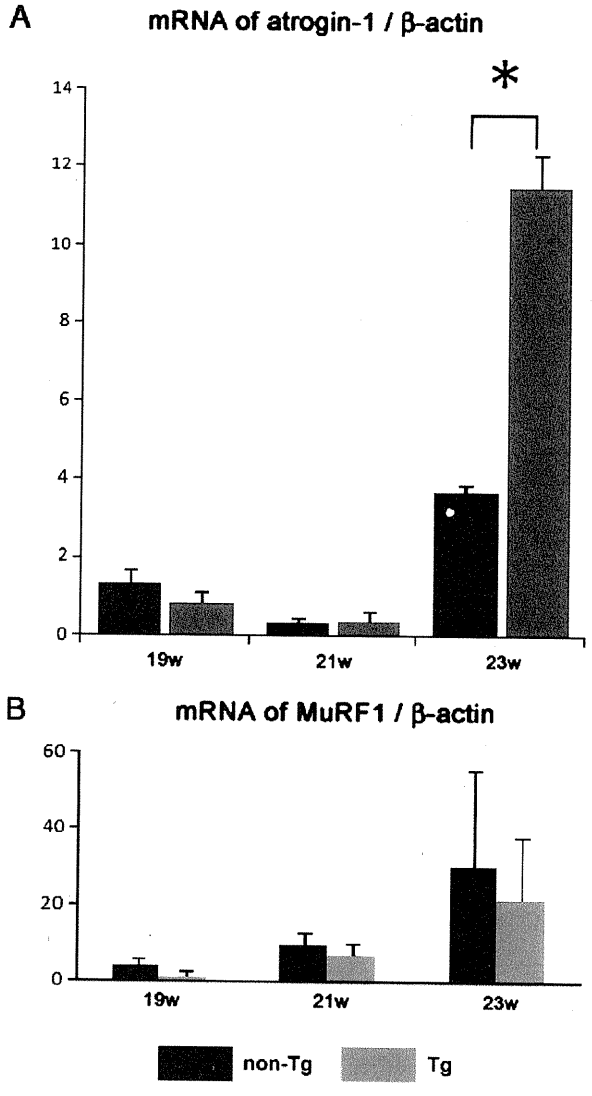

Fig. 6. Up-regulation of atrogin-1/MAFbx in the end stage of mutant SOD1 Tg mice. mRNA levels of ubiquitin ligases, atrogin-1 (A) and MuRF1 (B) ($n=5$) in Gc muscles were quantified by real time PCR. Mann–Whitney test, $^*p<0.05$.

cord. NO reacts rapidly with superoxide leading to the formation of peroxynitrite. nNOS, eNOS and 3-nitrotyrosine, which is a relative specific marker for peroxynitrite-mediated nitration, are selectively increased in the spinal motoneurons of sporadic and familial ALS [33]. Another study also suggested that 3-nitrotyrosine immunoreactivity is enhanced in the spinal motoneurons of sporadic and familial ALS [34].

On the other hand, there are few reports about nNOS in the skeletal muscles of ALS patients. Soraru et al. reported a reduced activity of respiratory chain complexes with mitochondrial encoded subunits and a lower nNOS amount in human ALS muscles [35]. In our study, nNOS dislocation had no relation to the extent of muscle atrophy or disease duration in this small sample size due to the variation of the disease course in human ALS. In the mutant SOD1 Tg mice model, we found increasing nNOS dislocation in the angulated muscle fibers during the disease course. In humans with ALS, we also found nNOS dislocation in the round abnormal fibers suggesting differences in the pathology between sporadic and familial ALS. In the mutant SOD1 Tg mice model, we found increasing nNOS dislocation during the disease course. We also found decreasing amounts of nNOS in the P fraction in the subcellular fractionation, suggesting the fragile connection of nNOS to the sarcolemma, although nNOS seemed to be located at the sarcolemma in the immunohistochemistry. The relatively small numbers of fibers represented by the cytosolic staining of nNOS may contribute to the comparable amount of nNOS bands in the S1 fraction of the Tg mice muscles and those of non-Tg littermates. As the mutant SOD1 Tg mice revealed the same amount of nNOS expression from the early phase of the disease, nNOS dislocation may be an upstream disease-modifying event of the muscle atrophy in the ALS pathology.

Previously, another group reported the beneficial effects of nNOS inhibition in models of motor neuron disease. Ikeda et al. reported that a nNOS inhibitor, 7-nitroindazole (7NI), potentiated grip strength and attenuated deformities in the forelimbs and reduced denervation muscle atrophy using a mouse model of motor neuron disease, Wobbler mice [36]. However, no improvement of the life span in Wobbler mice was observed. Facchinetti et al. reported that another nNOS inhibitor, ARL 17477, prolonged the survival in G93A-SOD1 Tg mice [37], but this drug is not available. Others failed to demonstrate the efficacy of nNOS in lengthening the survival of ALS Tg mice using three different nNOS inhibitors [37,38]. iNOS is abnormally expressed during the disease course of ALS, and may contribute to the unresponsiveness to nNOS inhibitors.

We previously examined the role of nNOS in denervation-induced muscle atrophy [24]. On the side denervated by cutting of the sciatic nerve, the muscle weight was significantly decreased 14 days after operation, and nNOS had already disappeared from the sarcolemma at 3 days after denervation. We observed much milder muscle atrophy in the denervated muscle of nNOS-null mice, as well as in mice injected with a nNOS inhibitor, 7-NI, or a pan-NOS inhibitor, N-(G)-nitro-L-arginine methyl ester (L-NAME) [24]. However, these drugs were revealed not to relieve the disease progression of ALS through intravenous and intranasal approaches [37,38]. Another water soluble nNOS-selective inhibitor, N5-(1-Imino-3-butenyl)-L-ornithine (L-VNIO), was proved to be active in an *in vivo* model of blood pressure [39–43]. L-VNIO may be beneficial in skeletal muscle and spinal cords in motor neuron diseases.

In conclusion, we demonstrated that nNOS dislocated from the sarcolemma to the cytoplasm may be the upstream disease-modifying event of muscle atrophy in human ALS and Tg mice. A common nNOS dislocation/atrogin-1 pathway among tail suspension, denervation and ALS induced muscle atrophy is suggested. nNOS modulation therapy may be beneficial in several types of muscle atrophy, but modulation of the drug delivery system and potentiation of the drug will be necessary.

Acknowledgements

This work was supported by Research grants from Nervous and Mental disorders (20B-13), Research on Measures for Intractable Diseases, Research on Psychiatric and Neurological Diseases and Mental Health from the Japanese Ministry of Health Labor and Welfare, Grants-in-Aids for Scientific Research (C: 19590977, 21591070) and Grants-in-Aids for Young Scientist (19890016) from the Japanese Ministry of Education, Culture, Sports, Science and Technology.

We thank Ms. N. Shimakura, K. Aihara, R. Ando, T. Nakatani, and M. Toyosawa for technical supports. We also thank Mr. Brent Bell for reading the manuscript.

References

[1] Mitchell JD, Borasio GD. Amyotrophic lateral sclerosis. Lancet 2007;369:2031–41.
[2] Miller TM, Smith RA, Cleveland DW. Amyotrophic lateral sclerosis and gene therapy. Nat Clin Pract Neurol 2006;2:462–3.
[3] Pasinelli P, Brown RH. Molecular biology of amyotrophic lateral sclerosis: insights from genetics. Nat Rev Neurosci 2006;7:710–23.

[4] Rosen DR, Siddique T, Patterson D, Figlewicz DA, Sapp P, Hentati A, et al. Mutations in Cu/Zn superoxide dismutase gene are associated with familial amyotrophic lateral sclerosis. Nature 1993;362:59–62.
[5] Aoki M, Abe K, Houi K, Ogasawara M, Matsubara Y, Kobayashi T, et al. Variance of age at onset in a Japanese family with amyotrophic lateral sclerosis associated with a novel Cu/Zn superoxide dismutase mutation. Ann Neurol 1995;37:676–9.
[6] Aoki M, Ogasawara M, Matsubara Y, Narisawa K, Nakamura S, Itoyama Y, et al. Mild ALS in Japan associated with novel SOD mutation. Nat Genet 1993;5:323–4.
[7] Nagai M, Aoki M, Miyoshi I, Kato M, Pasinelli P, Kasai N, et al. Rats expressing human cytosolic copper–zinc superoxide dismutase transgenes with amyotrophic lateral sclerosis: associated mutations develop motor neuron disease. J Neurosci 2001;21:9246–54.
[8] Sasaki S, Nagai M, Aoki M, Komori T, Itoyama Y, Iwata M. Motor neuron disease in transgenic mice with an H46R mutant SOD1 gene. J Neuropathol Exp Neurol 2007;66:517–24.
[9] Mizuno H, Warita H, Aoki M, Itoyama Y. Accumulation of chondroitin sulfate proteoglycans in the microenvironment of spinal motor neurons in amyotrophic lateral sclerosis transgenic rats. J Neurosci Res 2008;86:2512–23.
[10] Ishigaki A, Aoki M, Nagai M, Warita H, Kato S, Kato M, et al. Intrathecal delivery of hepatocyte growth factor from amyotrophic lateral sclerosis onset suppresses disease progression in rat amyotrophic lateral sclerosis model. J Neuropathol Exp Neurol 2007;66:1037–44.
[11] Tidball JG. Mechanical signal transduction in skeletal muscle growth and adaptation. J Appl Physiol 2005;98:1900–8.
[12] Ikemoto M, Nikawa T, Takeda S, Watanabe C, Kitano T, Baldwin KM, et al. Space shuttle flight (STS-90) enhances degradation of rat myosin heavy chain in association with activation of ubiquitin–proteasome pathway. FASEB J 2001;15: 1279–81.
[13] Bodine SC, Latres E, Baumhueter S, Lai VK, Nunez L, Clarke BA, et al. Identification of ubiquitin ligases required for skeletal muscle atrophy. Science 2001;294: 1704–8.
[14] Gomes MD, Lecker SH, Jagoe RT, Navon A, Goldberg AL. Atrogin-1, a muscle-specific F-box protein highly expressed during muscle atrophy. Proc Natl Acad Sci U S A 2001;98:14440–5.
[15] Bodine SC, Stitt TN, Gonzalez M, Kline WO, Stover GL, Bauerlein R, et al. Akt/mTOR pathway is a crucial regulator of skeletal muscle hypertrophy and can prevent muscle atrophy in vivo. Nat Cell Biol 2001;3:1014–9.
[16] Song YH, Li Y, Du J, Mitch WE, Rosenthal N, Delafontaine P. Muscle-specific expression of IGF-1 blocks angiotensin II-induced skeletal muscle wasting. J Clin Invest 2005;115:451–8.
[17] Rommel C, Bodine SC, Clarke BA, Rossman R, Nunez L, Stitt TN, et al. Mediation of IGF-1-induced skeletal myotube hypertrophy by PI(3)K/Akt/mTOR and PI(3)K/Akt/GSK3 pathways. Nat Cell Biol 2001;3:1009–13.
[18] Latres E, Amini AR, Amini AA, Griffiths J, Martin FJ, Wei Y, et al. Insulin-like growth factor-1 (IGF-1) inversely regulates atrophy-induced genes via the phosphatidylinositol 3-kinase/Akt/mammalian target of rapamycin (PI3K/Akt/mTOR) pathway. J Biol Chem 2005;280:2737–44.
[19] Cai D, Frantz JD, Tawa Jr NE, Melendez PA, Oh BC, Lidov HG, et al. IKKbeta/NF-kappaB activation causes severe muscle wasting in mice. Cell 2004;119:285–98.
[20] Sandri M, Sandri C, Gilbert A, Skurk C, Calabria E, Picard A, et al. Foxo transcription factors induce the atrophy-related ubiquitin ligase atrogin-1 and cause skeletal muscle atrophy. Cell 2004;117:399–412.
[21] Li YP, Schwartz RJ, Waddell ID, Holloway BR, Reid MB. Skeletal muscle myocytes undergo protein loss and reactive oxygen-mediated NF-kappaB activation in response to tumor necrosis factor alpha. FASEB J 1998;12:871–80.
[22] Acharyya S, Butchbach ME, Sahenk Z, Wang H, Saji M, Carathers M, et al. Dystrophin glycoprotein complex dysfunction: a regulatory link between muscular dystrophy and cancer cachexia. Cancer Cell 2005;8:421–32.
[23] Acharyya S, Ladner KJ, Nelsen LL, Damrauer J, Reiser PJ, Swoap S, et al. Cancer cachexia is regulated by selective targeting of skeletal muscle gene products. J Clin Invest 2004;114:370–8.
[24] Suzuki N, Motohashi N, Uezumi A, Fukada S, Yoshimura T, Itoyama Y, et al. NO production results in suspension-induced muscle atrophy through dislocation of neuronal NOS. J Clin Invest 2007;117:2468–76.
[25] Koyama S, Arawaka S, Chang-Hong R, Wada M, Kawanami T, Kurita K, et al. Alteration of familial ALS-linked mutant SOD1 solubility with disease progression: its modulation by the proteasome and Hsp70. Biochem Biophys Res Commun 2006;343:719–30.
[26] Kato M, Aoki M, Ohta M, Nagai M, Ishizaki F, Nakamura S, et al. Marked reduction of the Cu/Zn superoxide dismutase polypeptide in a case of familial amyotrophic lateral sclerosis with the homozygous mutation. Neurosci Lett 2001;312:165–8.
[27] Aoki M, Kato S, Nagai M, Itoyama Y. Development of a rat model of amyotrophic lateral sclerosis expressing a human SOD1 transgene. Neuropathology 2005;25: 365–70.
[28] Sasaki S, Aoki M, Nagai M, Kobayashi M, Itoyama Y. Mitochondrial alterations in transgenic mice with an H46R mutant Cu/Zn superoxide dismutase gene. J Neuropathol Exp Neurol 2009;68:365–73.
[29] Brenman JE, Chao DS, Xia H, Aldape K, Bredt DS. Nitric oxide synthase complexed with dystrophin and absent from skeletal muscle sarcolemma in Duchenne muscular dystrophy. Cell 1995;82:743–52.
[30] Leger B, Vergani L, Soraru G, Hespel P, Derave W, Gobelet C, et al. Human skeletal muscle atrophy in amyotrophic lateral sclerosis reveals a reduction in Akt and an increase in atrogin-1. FASEB J 2006;20:583–5.
[31] Kato N, Sato S, Yokoyama H, Kayama T, Yoshimura T. Sequential changes of nitric oxide levels in the temporal lobes of kainic acid-treated mice following application of nitric oxide synthase inhibitors and phenobarbital. Epilepsy Res 2005;65:81–91.
[32] Kim SF, Huri DA, Snyder SH. Inducible nitric oxide synthase binds, S-nitrosylates, and activates cyclooxygenase-2. Science 2005;310:1966–70.
[33] Beal MF, Ferrante RJ, Browne SE, Matthews RT, Kowall NW, Brown Jr RH. Increased 3-nitrotyrosine in both sporadic and familial amyotrophic lateral sclerosis. Ann Neurol 1997;42:644–54.
[34] Cassina P, Peluffo H, Pehar M, Martinez-Palma L, Ressia A, Beckman JS, et al. Peroxynitrite triggers a phenotypic transformation in spinal cord astrocytes that induces motor neuron apoptosis. J Neurosci Res 2002;67:21–9.
[35] Soraru G, Vergani L, Fedrizzi L, D'Ascenzo C, Polo A, Bernazzi B, et al. Activities of mitochondrial complexes correlate with nNOS amount in muscle from ALS patients. Neuropathol Appl Neurobiol 2007;33:204–11.
[36] Ikeda K, Iwasaki Y, Kinoshita M. Neuronal nitric oxide synthase inhibitor, 7-nitroindazole, delays motor dysfunction and spinal motoneuron degeneration in the Wobbler mouse. J Neurol Sci 1998;160:9–15.
[37] Facchinetti F, Sasaki M, Cutting FB, Zhai P, MacDonald JE, Reif D, et al. Lack of involvement of neuronal nitric oxide synthase in the pathogenesis of a transgenic mouse model of familial amyotrophic lateral sclerosis. Neuroscience 1999;90: 1483–92.
[38] Martinez JA, Francis GJ, Liu WQ, Pradzinsky N, Fine J, Wilson M, et al. Intranasal delivery of insulin and a nitric oxide synthase inhibitor in an experimental model of amyotrophic lateral sclerosis. Neuroscience 2008;157:908–25.
[39] Talman WT, Dragon DN. Transmission of arterial baroreflex signals depends on neuronal nitric oxide synthase. Hypertension 2004;43:820–4.
[40] Yamaleyeva LM, Gallagher PE, Vinsant S, Chappell MC. Discoordinate regulation of renal nitric oxide synthase isoforms in ovariectomized mRen2.Lewis rats. Am J Physiol Regul Integr Comp Physiol 2007;292:R819–26.
[41] Kakoki M, Zou AP, Mattson DL. The influence of nitric oxide synthase 1 on blood flow and interstitial nitric oxide in the kidney. Am J Physiol Regul Integr Comp Physiol 2001;281:R91–7.
[42] Babu BR, Griffith OW. N5-(1-Imino-3-butenyl)-L-ornithine. A neuronal isoform selective mechanism-based inactivator of nitric oxide synthase. J Biol Chem 1998;273:8882–9.
[43] Burkard N, Rokita AG, Kaufmann SG, Hallhuber M, Wu R, Hu K, et al. Conditional neuronal nitric oxide synthase overexpression impairs myocardial contractility. Circ Res 2007;100:e32–44.

Cell Transplantation, Vol. 20, pp. 727–739, 2011
Printed in the USA.

0963-6897/11 $90.00 + .00
DOI: 10.3727/096368910X536554
E-ISSN 1555-3892
www.cognizantcommunication.com

Comparative Study of Methods for Administering Neural Stem/Progenitor Cells to Treat Spinal Cord Injury in Mice

Yuichiro Takahashi,*† Osahiko Tsuji,* Gentaro Kumagai,‡ Chikako Miyauchi Hara,† Hirotaka James Okano,† Atsushi Miyawaki,§¶ Yoshiaki Toyama,* Hideyuki Okano,† and Masaya Nakamura*

*Department of Orthopaedic Surgery, School of Medicine, Keio University, Tokyo, Japan
†Department of Physiology, School of Medicine, Keio University, Tokyo, Japan
‡Department of Orthopaedic Surgery, School of Medicine, Hirosaki University, Aomori, Japan
§Laboratory for Cell Function and Dynamics, Advanced Technology Development Group, Brain Science Institute, RIKEN, Saitama, Japan
¶Life Function and Dynamics, ERATO, JST, Saitama, Japan

To investigate potential cures for spinal cord injury (SCI), several researchers have transplanted neural stem/progenitor cells (NS/PCs) into the injured spinal cord by different procedures, including intralesional (IL), intrathecal (IT), and intravenous (IV) injection. However, there are no reports quantifying or comparing the number of cells successfully transplanted to the lesion site by each procedure in vivo. The purpose of the present study was to determine the optimal method of cell transplantation to the SCI site in terms of grafted cell survival and safety. For this purpose, we developed mouse NS/PCs that expressed a novel Venus-luciferase fusion protein that enabled us to detect a minimum of 1,000 grafted cells in vivo by bioluminescence imaging (BLI). After inducing contusive SCI at the T10 level in mice, NS/PCs were transplanted into the injured animals three different ways: by IL, IT, or IV injection. Six weeks after the transplantation, BLI analysis showed that in the IL group, the luminescence intensity of the grafted cells had decreased to about 10% of its initial level, and appeared at the site of injury. In the IT group, the luminescence of the grafted cells, which was distributed throughout the entire subarachnoid space immediately after transplantation, was detected at the injured site 1 week later, and by 6 weeks had gradually decreased to about 0.3% of its initial level. In the IV group, no grafted cells were detected at the site of injury, but all of these mice showed luminescence in the bilateral chest, suggesting pulmonary embolism. In addition, one third of these mice died immediately after the IV injection. In terms of grafted cell survival and safety, we conclude that the IL application of NS/PCs is the most effective and feasible method for transplanting NS/PCs into the SCI site.

Key words: Spinal cord injury (SCI); Transplantation; Neural stem/progenitor cells (NS/PCs); Bioluminescence imaging (BLI)

INTRODUCTION

Because the adult central nervous system (CNS) has little potential for regeneration, spinal cord injury (SCI) usually results in severe damage, leading to paraplegia, tetraplegia, or worse. Several strategies have been used to develop new therapies that would allow patients to regain the use of their paralyzed limbs. Because cell transplantation is one of the potential therapies, various kinds of cells have been used as the transplantation source for SCI (14,18,32–34,37,38,46). Among them, neural stem/progenitor cell (NS/PC) transplantation is considered one of the most promising, because the transplantation of NS/PCs into rodent SCI models (13,15,27,42, 44,48) and of human neural stem/progenitor cells (NS/PCs) into a marmoset SCI model (28) have been shown to promote functional recovery.

From the viewpoint of clinical trials, it is critical to determine how best to apply cells to the injured spinal cord. Three application methods for cell transplantation for SCI are used: intralesional (IL), intrathecal (IT), and intravenous (IV). Some previous studies have sought to

Received February 18, 2010; final acceptance September 24, 2010. Online prepub date: November 5, 2010.
Address correspondence to Masaya Nakamura, Department of Orthopaedic Surgery, School of Medicine, Keio University, 35 Shinanomachi, Shinjuku, Tokyo 160-8582, Japan. Tel: +81-3-3353-1211; Fax: +81-3353-6597; E-mail: masa@sc.itc.keio.ac.jp *or* Hideyuki Okano, Department of Physiology, School of Medicine, Keio University, 35 Shinanomachi, Shinjuku, Tokyo 160-8582, Japan. Tel: +81-3-5363-3747; Fax: +81-3-3357-5445; E-mail: hidokano@sc.itc.keio.ac.jp

compare different cell transplantation methods for treating SCI. For example, the IL application of NS/PCs was reported to be more effective than the IT application (43), and the IV application of NS/PCs more effective than the IL application (10). However, these reports are not directly comparable, because they did not use the same number of cells for the initial transplants. Previous reports using other kinds of cells for transplantation showed that the IL application was more effective than IT or IV for introducing cells to the SCI site (7,18,67), and that IT was more effective than IV (6,54). However, the number of cells transplanted by each method was not quantified or compared for the different methods in vivo, and the safety of the different methods was not compared. Moreover, some reports did not use uniform numbers of cells for the initial transplantation or examine the grafted cells in vivo over the long term. Therefore, it has remained unclear which application of NS/PCs is best for injured spinal cord in terms of cell survival and safety.

In the present study, to determine the best way to transplant NS/PCs into the SCI site, we applied NS/PCs to the mouse injured spinal cord by IL, IT, or IV injection, and quantitatively examined the survival and distribution of the grafted cells, as well as the complications associated with NS/PC transplantation, such as tumor formation and pulmonary embolism. For this purpose, we developed a new reporter gene for bioluminescence imaging (BLI), which enabled us to quantify the bioluminescent signals of small numbers of cells in vivo over time.

MATERIALS AND METHODS

Lentiviral Vector Expressing the ffLuc Reporter Gene

A novel fusion HIV-1-based lentiviral vector, expressing ffLuc under the EF1α promoter (see Fig. 1A) (Hara et al., in preparation), was used in this study. ffLuc is composed of Venus and Luc2: Venus is a kind of yellow fluorescence protein (40), Luc2 is firefly (*Photinus pyralis*)-derived luciferase. The luciferase gene fragment was excised from the pGL4-Basic vector (Promega, Madison, WI). This vector enabled the detection of grafted cells as strong bioluminescent signals from ffLuc in live SCI mice and as fluorescent signals in spinal cord sections. Twenty-four hours before the transfection, 293T cells were seeded into poly-L-lysine-coated T175 flasks. The cells were transfected using the lipofection protocol for the FuGENE6 transfection reagent (Roche, Indianapolis, IN). Three days after transfection, the conditioned medium was collected, and the virus was concentrated by centrifugation at 25,000 rpm for 1.5 h at 4°C. The pelleted viral particles were resuspended and stored frozen at –80°C. The titer of the concentrated virus was 1×10^8 to 2×10^8 transducing units per milliliter (TU/ml) when assayed using 293T cells, and the infectivity was determined by fluorescence expression as analyzed on a FACS Calibur (Becton-Dickinson, Franklin, Lakes, NJ).

NS/PC Labeling and Differentiation Assay

NS/PCs were cultured as reported previously (55). In brief, the striatum of a C57BL/6J mouse on embryonic day 14 was dissociated using a fire-polished glass pipette, and the dissociated cells were collected by centrifugation and resuspended in culture medium. The culture medium consisted of DMEM/F12 supplemented with a hormone mixture as described previously (55). Human recombinant fibroblast growth factor-2 (FGF-2) and epidermal growth factor (EGF) (20 ng/ml each) were added every 2 days. The cells formed floating cell clusters (neurospheres) within 2–3 days. The concentrated virus was added to the culture medium to infect primary NS/PCs (multiplicity of infection, MOI = 1.0). After being propagated for two passages, the neurospheres were used for in vivo BLI or dissociated into single cells and plated onto poly-L-ornithine-coated coverslips at a density of 1×10^5 cells/ml for in vitro analysis. The virally transduced NS/PCs were allowed to differentiate for 5 days and were fixed with 4% paraformaldehyde in 0.1 M phosphate-buffered saline (PBS) for immunocytochemistry.

SCI Model

Adult female C57BL/6J mice (20–22 g, $n = 20$; Clea, Tokyo, Japan) were anesthetized with an IP injection of ketamine (100 mg/kg) and xylazine (10 mg/kg). After laminectomy at the 10th thoracic spinal vertebra (T10), the dorsal surface of the dura matter was exposed, and SCI was induced using a commercially available SCI device (IH impactor, Precision Systems and Instrumentation, Lexington, KY), as described previously (47). This device creates a reliable contusion injury by rapidly applying a force-defined impact (60 kdyn) with a stainless steel-tipped impactor. All procedures were approved by the ethics committee of Keio University, and were in accordance with the Guide for the Care and Use of Laboratory Animals.

NS/PC Transplantation

The lentivirally transduced NS/PCs were transplanted into each mouse immediately after SCI using one of the three different methods: IL cell transplantation (IL group, $n = 5$), IT cell transplantation (IT group, $n = 5$), and IV cell transplantation (IV group, $n = 10$). For the IL group, the tip of a glass micropipette was inserted into the epicenter of the injured spinal cord, and the NS/PCs were

injected through it. For the IT group, a laminectomy was performed at the L3 level, and the NS/PCs were injected into the subarachnoid space at the same level, through a 32-gauge catheter. For the IV group, the NS/PCs were injected into the tail vein or femoral vein through a 32-gauge catheter. For all the applications, the number and concentration of the transplanted cells were the same (5×10^5 cells/2 μl), and the NS/PCs were injected at a rate of 1 μl/min with a Hamilton syringe (25 μl) and stereotaxic microinjector (KDS 310, Muromachi-kikai, Tokyo, Japan). The number of viable cells in the suspensions was determined by cell counting using trypan blue dye and by the signal intensity of the NS/PCs determined by BLI prior to transplantation.

Bioluminescence Imaging

The Xenogen-IVIS 100 cooled CCD optical macroscopic imaging system (SC BioScience, Tokyo, Japan) (56) was used for BLI. Both in vitro and in vivo BLI was performed as previously reported (47). In brief, the signal intensity of the lentivirally transduced NS/PCs in vitro was examined on cells plated at various densities (approximate range 1×10^2 to 10^6 cells/10 μl) and the bioluminescent images were captured immediately after the addition of D-luciferin [D-(−)-2-(6′-hydroxy-2′-benzothiazolyl) thiazone-4-carboxylic acid] (15 mg/ml). In vivo BLIs were captured 15 min after the IP injection of D-luciferin (0.3 mg/g body weight) with the field-of-view set at 10 cm; because the photon count was most stable with its peak intensity between 10 and 30 min after the IP injection of D-luciferin. The integration time was fixed at 5 min for each image. All images were analyzed with the Igor (WaveMetrics, Lake Oswego, OR) and Living Image software (Xenogen, Alameda, CA), and the optical signal intensity was expressed as photon-flux (photon count), in units of photons/s/cm^2/steradian. Each image was displayed as a pseudocolored photon count image superimposed on a gray scale anatomic image. To quantify the measured light, we defined regions of interest (ROI) over the cell-implanted area and examined all values in the same ROI.

Immunohistochemistry

Animals were anesthetized and transcardially perfused with 4% paraformaldehyde in 0.1 M PBS 6 weeks after the transplantation. The spinal cord was removed, embedded in OCT compound, frozen in liquid nitrogen, and sagittally sectioned at 30 μm on a cryostat. For immunofluorescence staining, cultured cells or tissue sections were stained with primary antibodies, including anti-green fluorescence protein (GFP) (1:500; MBL, Woburn, MA), anti-glial fibrillary acid protein (GFAP) (1:500; AIC, Long Beach, CA), anti-β-III-tubulin (Tuj-1) (1:200; Sigma, St. Louis, MO), anti-2′,3′-cyclic nucleotide 3′-phosphodiesterase (CNPase) (1:200; Sigma), anti-Hu (1:1000; a gift from Dr. Robert Darnell, The Rockefeller University), and anti-APC (CC-1) (1:200; Oncogene, Cambridge, MA). Hoechst 33342 was used to counterstain the nuclei (Molecular Probes, Eugene, OR) and then samples were incubated with Alexa Fluor-conjugated secondary antibodies (1:500; Molecular Probes, Eugene, OR). Images were obtained by fluorescence microscopy (Axiocam; Carl Zeiss, Munich, Germany) or confocal microscopy (LSM700; Carl Zeiss). For diaminobenzidine staining, the sections were incubated at 4°C with anti-GFP (1:500; MBL), followed by biotinylated secondary antibodies (1:500; Jackson Immunoresearch). Biotinylated antibodies were visualized using the Vectastain Elite ABC kit (Vector Laboratories, Burlingame, CA), followed by diaminobenzidine (Sigma). Quantitative analysis of the NS/PCs after their differentiation in vitro was performed as described previously (47).

RESULTS

In Vitro Imaging and Differentiation Assay of Lentivirally Transduced NS/PCs

To identify and monitor the transplanted cells, NS/PCs were labeled by lentiviral infection with ffLuc expressed under the EF1α promoter (Fig. 1A). Owing to the stable and strong emission of ffLuc, which is a fusion protein of Venus and luciferase [(39), Hara et al., in preparation] we could observe the fluorescent signals of the Venus by fluorescence microscopy (Fig. 1B) and the bioluminescent signals of luciferase with BLI (Fig. 1C). FACS Calibur analysis revealed that >70% of these cells were positive for Venus (data not shown). The minimum number of cells that could be measured by their photon counts with BLI was approximately 100 cells in vitro. There was a linear correlation between the number of labeled cells and the photon count (Fig. 1D). The NS/PCs expressing ffLuc showed about 10 times stronger bioluminescence intensity in vitro than the reported intensity of NS/PCs expressing conventional luciferase with IRES-Venus (47). To confirm that the lentiviral transduction did not alter the properties of the NS/PCs, we performed differentiation assays on transduced NS/PCs. The transfected NS/PCs could be maintained and passaged using the conventional neurosphere method, and an in vitro differentiation assay revealed that the trasduced NS/PCs differentiated into Tuj1-positive (21.1 ± 2.1%), GFAP-positive (50.0 ± 2.8%), and CNPase-positive (17.9 ± 8.1%) cells (Fig. 1E–H), which are markers for neurons, astrocytes, and oligodendrocytes, respectively. These results showed the lentivirus-transduced NS/PCs had a similar multipotency to that reported for nontransduced NS/PCs (47).

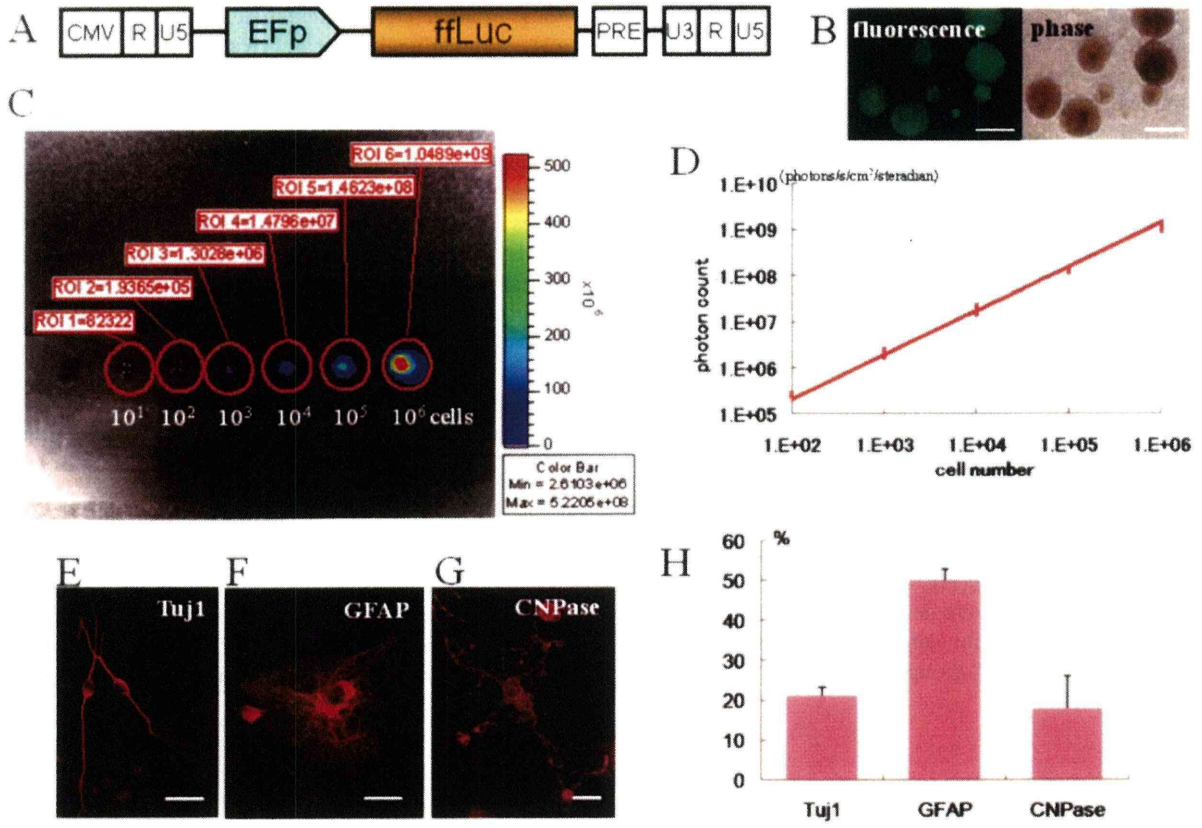

Figure 1. In vitro imaging and differentiation of lentivirally transduced NS/PCs. (A) Structure of the HIV-1-based lentivirus vector that expresses ffLuc under the elongation factor (EF)-1α promoter. (B) Fluorescent (left) and phase-contrast (right) images of neurospheres derived from ffLuc-expressing NS/PCs. (C) The ffLuc-expressing NS/PCs showed strong luciferase intensity. (D) There was a linear correlation between the number of labeled NS/PCs and their photon count in vitro. Data are the mean ± SEM; $n = 10$. (E–G) The ffLuc-expressing NS/PCs differentiated into Tuj1-positive (E), GFAP-positive (F), and CNPase-positive (G) cells. (H) Quantitative analysis of the ffLuc-expressing NS/PC phenotype after differentiation. Data are the mean ± SEM; $n = 3$. Scale bars: 200 μm (B), 20 μm (E–G).

Detection Limits for In Vivo Imaging of NS/PCs Transplanted Into Intact Spinal Cord

When transplanted into the intact spinal cord of adult C57BL/6 mice, the transfected NS/PCs showed one tenth of the photon count that was observed in vitro (Fig. 2A). There was a linear correlation between the numbers of grafted cells and the photon count in vivo (Fig. 2B), and the minimum number of grafted cells that could be measured with BLI was approximately 1,000 cells (Fig. 2C). As few as 100 grafted cells could be detected as bioluminescence in the normal spinal cord after opening the skin at the transplantation site (Fig. 2D).

In Vivo Imaging of NS/PCs Grafted Into the Injured Spinal Cord

To examine the survival and distribution of the transplanted cells in vivo, the photon counts of the grafted cells in each mouse were measured weekly by BLI for 6 weeks after transplantation. In the IL group, the photon counts of the grafted cells were detected at the lesion site for all 6 weeks, in spite of their decrease to approximately 30% of the initial level at 7 days and to 9.4 ± 0.03% at 6 weeks after the transplantation (Fig. 3A, B). In the IT group, the grafted cells were distributed along the entire subarachnoid space immediately after transplantation, and some were detected at the lesion site 7 day later. The bioluminescence of the grafted cells at the lesion site gradually disappeared thereafter. The photon counts of the grafted cells also decreased, to about 5% of the initial level at 1 week and 0.3 ± 0.0%, which is almost background measurement value, at 6 weeks after transplantation (Fig. 3C, D). In the IV group, no bioluminescence was detected at either the site of injury or in the uninjured spinal cord at any of the time points examined (Fig. 3E, F). In contrast, strong biolumines-

cence was observed in the bilateral chest immediately after the injection of the NS/PCs in all 10 animals of the IV group (Fig. 3G), and 3 of the 10 animals died immediately after the injection. In these mice, we confirmed the strong bioluminescence of the grafted cells in the lung (Fig. 3H). Although the luminescence in the bilateral chest became undetectable the next day in the surviving mice, two of the other seven mice died within 4 days of the transplantation. Five of the original 10 mice in the IV group survived for the full 6 weeks following the cell injection.

Immunohistochemistry

To examine the survival and distribution of the grafted cells histologically, immunohistochemistry with an anti-GFP antibody, which could detect ffLuc protein, was performed 6 weeks after transplantation to identify the ffLuc-positive grafted cells. Among the three groups, the IL group showed the best survival of ffLuc-positive cells at the lesion site (Fig. 4A, B). In the IT group, only a few grafted cells were detected at the lesion site (Fig. 4C, D). We could not detect any grafted cells at the lesion site in the IV group (Fig. 4E, F). In IL group, these grafted cells differentiated into neurons, astrocytes, and oligodendrocytes within the injured spinal cord (Fig. 4G–I), as previously reported (47). In the IT group, there were some ffLuc-positive cell clusters that lay on the surface of the spinal cord (Fig. 5A, C, D) and the cauda equina (Fig. 5B, E, F). These cells, which also differentiated into neurons, astrocytes, and oligodendrocytes (Fig. 5G–I), attached on the surface of pia matter of the uninjured spinal cord, but not invaded into the spinal cord tissue (Fig. 5C–F). In the IV group, ffLuc-positive cells were observed in the lung and spleen, and GFP-positive fragments were found in the glomeruli of the kidney (Fig. 6), although no ffLuc-positive cells were detected at the lesion site. There was no tumor formation, at least 6 weeks after transplantation, in any of the three groups.

DISCUSSION

In the present study we used a new reporter gene, ffLuc, and BLI for the longitudinal tracking and quantification of grafted cells in vivo. Our findings demonstrated that the IL injection of NS/PCs resulted in the best survival of the grafted cells among the three appli-

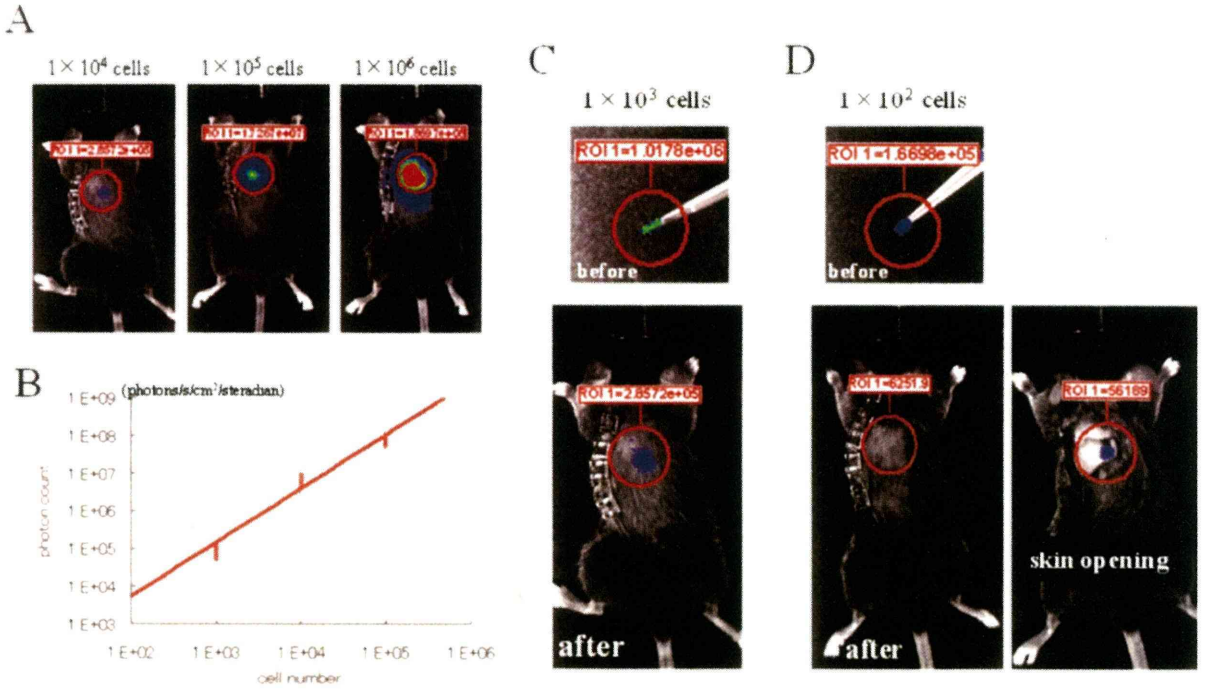

Figure 2. In vivo imaging of the grafted NS/PCs in the intact spinal cord. (A) Luminescence of the grafted NS/PCs was detected in vivo. In vivo, their photon counts were approximately one tenth of those observed in vitro. (B) There was a linear correlation between the number of grafted NS/PCs and the photon count in vivo. Data are the mean ± SEM; $n = 3$. (C) The luminescence of 1,000 cells transplanted into the normal spinal cord was detectable by photon count. (D) The luminescence of 100 cells grafted into the normal spinal cord was undetectable without opening the skin.

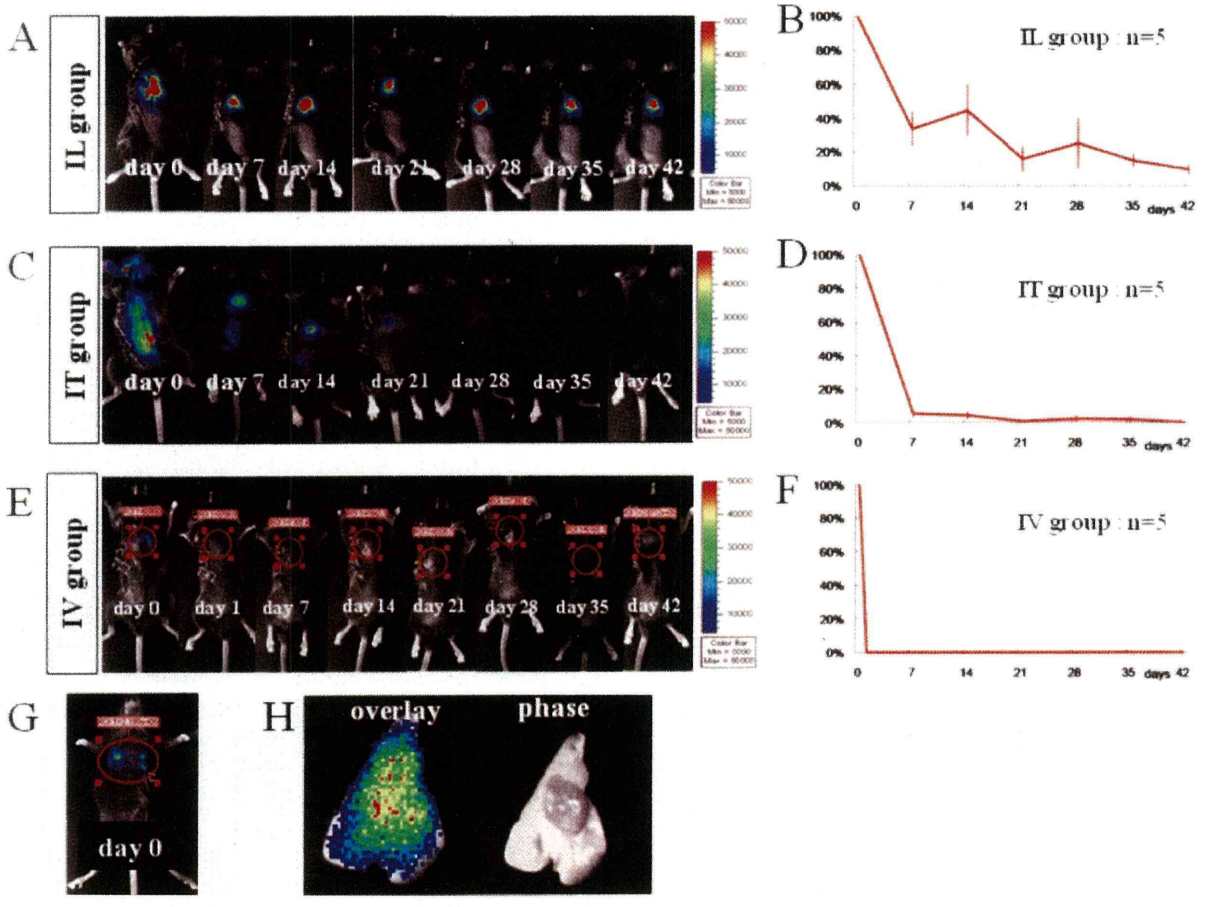

Figure 3. (A, C, E) Representative in vivo images of NS/PCs transplanted by the three application methods: (A) IL group, (C) IT group, and (E) IV group. (B, D, F) Quantitative analysis of the photon counts of the grafted NS/PCs in the IL group (B), IT group (D), and IV group (F). Data are the mean ± SEM; $n = 5$. (G) Strong luminescence was observed in the bilateral chest immediately after transplantation in all 10 animals of the IV group. (H) A resected lung from the IV group showed strong luminescence from the transplanted cells.

cations, and no complications were seen in the recipient mouse. Our analysis also revealed the distribution of the cells transplanted by the three methods.

To analyze the kinetics of cells after their transplantation in vivo, several previous studies have used immunohistochemistry, gamma scintigraphic imaging (1,11,20, 24), and magnetic resonance imaging (MRI) (3,26,29, 53). However, none of these methods permit the quantitative and continuous evaluation of the transplanted cells. Immunohistochemical analysis cannot track the fate of grafted cells in the same animal, because the animals need to be sacrificed at serial posttransplant time points to examine the grafted cells. Scintigraphic imaging using a radioactive tracer to label grafted cells enables the examination of their survival and distribution in vivo, but they can only be observed for a short time, owing to the tracer's short half-life and the dilution effect by cell division. MRI can detect the distribution of the transplanted cells at their initial deposition with high sensitivity, but the MRI signals from dead cells cannot be distinguished from those of live signals, which diminishes the usefulness of this method over time.

To overcome these problems, we used a BLI system, which enabled us to trace only living grafted cells in the same animal at multiple time points and to quantify the bioluminescence intensity of the grafted cells as a photon count (17,22,25,35,56,60,66). Although there are previous reports in which grafted cells were analyzed by BLI in injured spinal cord (33,47), the intensity of the bioluminescence in those studies was not strong enough to detect small numbers of cells. In the present study, we used a novel fusion protein, ffLuc. NS/PCs express-

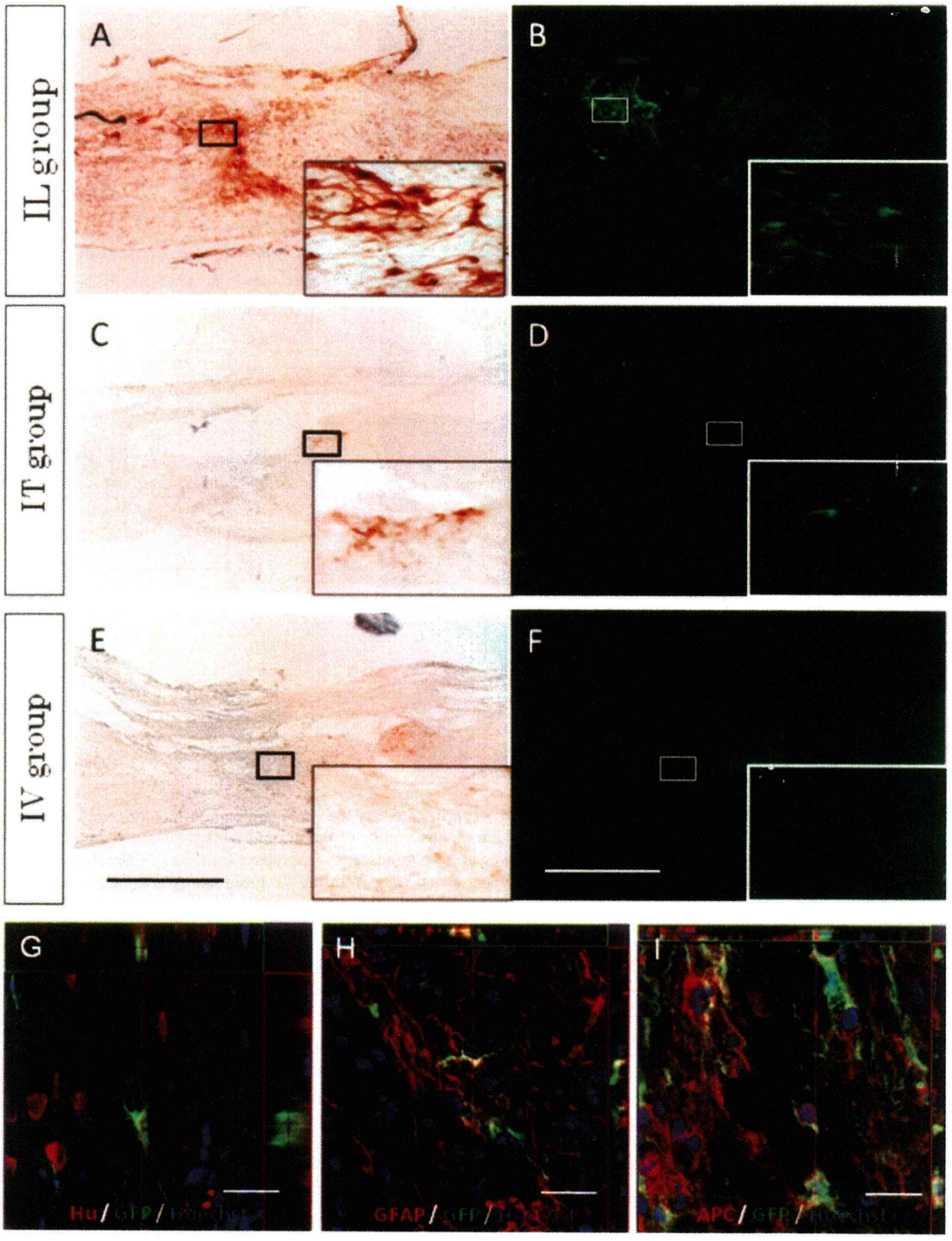

Figure 4. Immunohistochemical analysis of the injured spinal cord 6 weeks after transplantation. The grafted cells were identified as ffLuc-positive cells by diaminobenzidine (A, C, E) and immunofluorescence (B, D, F) staining. (A, B) In the IL group, the grafted cells survived well at the lesion site. (C, D) In the IT group, a few grafted cells survived, and some were present at the surface of the lesion site. (E, F) In the IV group, no grafted cells could be detected at the lesion site. (G, H, I) In the IL group, the grafted cells differentiated into Hu-positive (G), GFAP-positive (H) and APC-positive (I) cells within the injured spinal cord. Scale bars: 500 μm at magnification 25×, inset at magnification 400× (A–F); 20 μm (G–I).

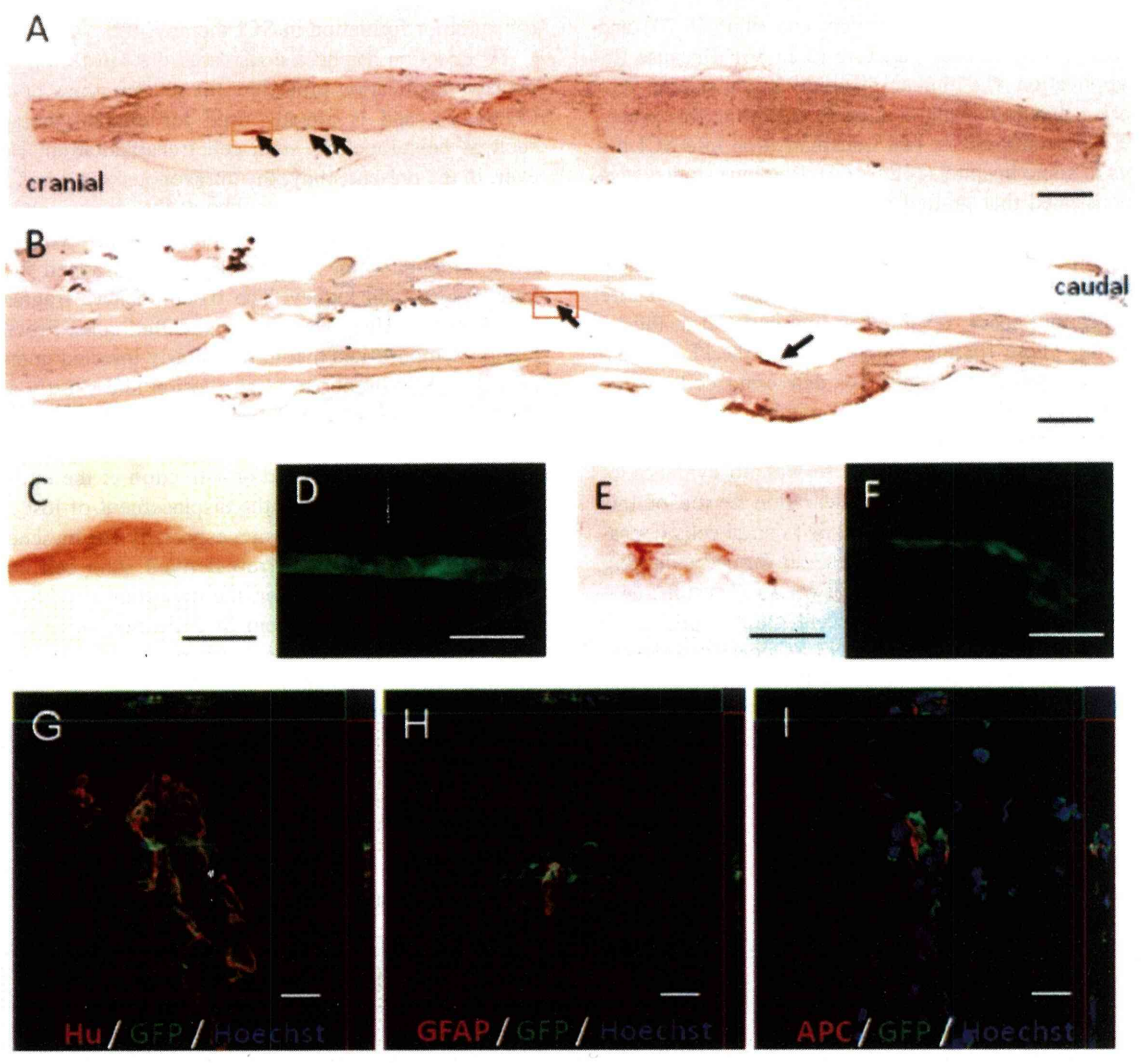

Figure 5. Immunohistochemical analysis of the IT group. (A, B) The grafted cells (arrow) were distributed on the surface of the uninjured spinal cord (A) and the cauda equina at 6 weeks after transplantation (B). (C, D) High magnification of the box in (A); the grafted cells were attached to the spinal cord surface, as shown by diaminobenzidine (C) and immunofluorescence (D) staining. (E, F) High magnification of the box in (B); the grafted cells were attached to the cauda equina, as shown by diaminobenzidine (E) and immunofluorescence (F) staining. (G, H, I) In the IT group, few grafted cells survived and differentiated into Hu-positive (G), GFAP-positive (H), and APC-positive (I) cells on the surface of the uninjured spinal cord and the cauda equina. Scale bars: 500 μm (A, B), 100 μm (C–F), 20 μm (G–I).

ing ffLuc emitted bioluminescent signals almost 10 times stronger than those of NS/PCs expressing conventional luciferase with IRES-Venus (47), thus enabling the detection of the bioluminescent signals of transplanted NS/PCs, even though they were present in small number or deep inside the mouse body. Because the ffLuc that is transfected by lentivirus is expressed in the NS/PCs permanently, we can trace the grafted NS/PCs accurately for a long period after transplantation.

From the viewpoint of clinical trials for cell transplantation to treat SCI, there is concern about causing additional damage to the injured spinal cord during the cell transplantation procedure. However, several researchers who have performed IL cell transplantation for SCI demonstrated that motor function is not degraded by the IL application (16); rather, the transplantation of cells by IL injection promotes functional recovery (19, 30,33,42,44,47).

The IT application is performed in two ways: one is by injection into the fourth ventricle (4,45,69,70) and the other is by lumbar puncture (5,21,36). Because the IT application via lumbar puncture is considered less invasive than transplantation by IL injection, this procedure has been used for cell transplantation into SCI patients in some hospitals (12,59,64). Previous studies also demonstrated that grafted NS/PCs transplanted through an IT application survive within the injured spinal cord (4,36,69). In the present study, however, cells transplanted by IT initially dispersed throughout the entire subarachnoid space, resulting in low survival at the lesion site. These findings suggested that the IT application is an uncertain method for delivering cells to the site of injury. Moreover, a small number of the grafted cells survived on the surface of the uninjured spinal cord and cauda equina. Although there was no evidence of tumor formation during the observation period of this study, it was previously reported that neural cells deposited at uninjured spinal cord sites had formed enlarging clusters of cells within a couple of weeks after transplantation (4). Furthermore, in a recent clinical procedure using an IT application, human NS/PCs caused a donor-derived brain tumor in a patient with ataxia telangiectasia, which was associated with comprised immunity (2). Therefore, it is highly likely that intrathecally applied cells adhering to the surface of the spinal cord could cause tumor formation in SCI therapy, too.

IV injection has been considered the most minimally invasive application procedure for several types of cells (31,61,63), and is already used for clinical therapies such as hematopoietic stem cell transplantation. However, in the present study, the intravenously injected NS/PCs were distributed throughout the body, and no grafted cells were detected within the injured spinal cord, although some grafted cells were trapped in the lung, spleen, and kidney. The ffLuc-positive fragments found in the kidney were broken grafted cells. Previous reports demonstrated that intravenously injected nonneural cells could be observed at a lesion site shortly after the transplantation, and the mechanisms for functional recovery in this situation are thought to be trophic support of the grafted cells and/or activation of the intrinsic neuronal cells, rather than the displacement of lost neurons and glia at the lesion site, especially for mesenchymal stem cell or bone-marrow-derived stem cell transplantation (52,62). However, the important mechanisms for functional recovery from SCI are not only trophic support, but also neural circuit reconstruction, axonal induction, and remyelination (8,50,65). The cells grafted into the host spinal cord play a role in maintaining the improved performance. Cummings et al. showed that se-

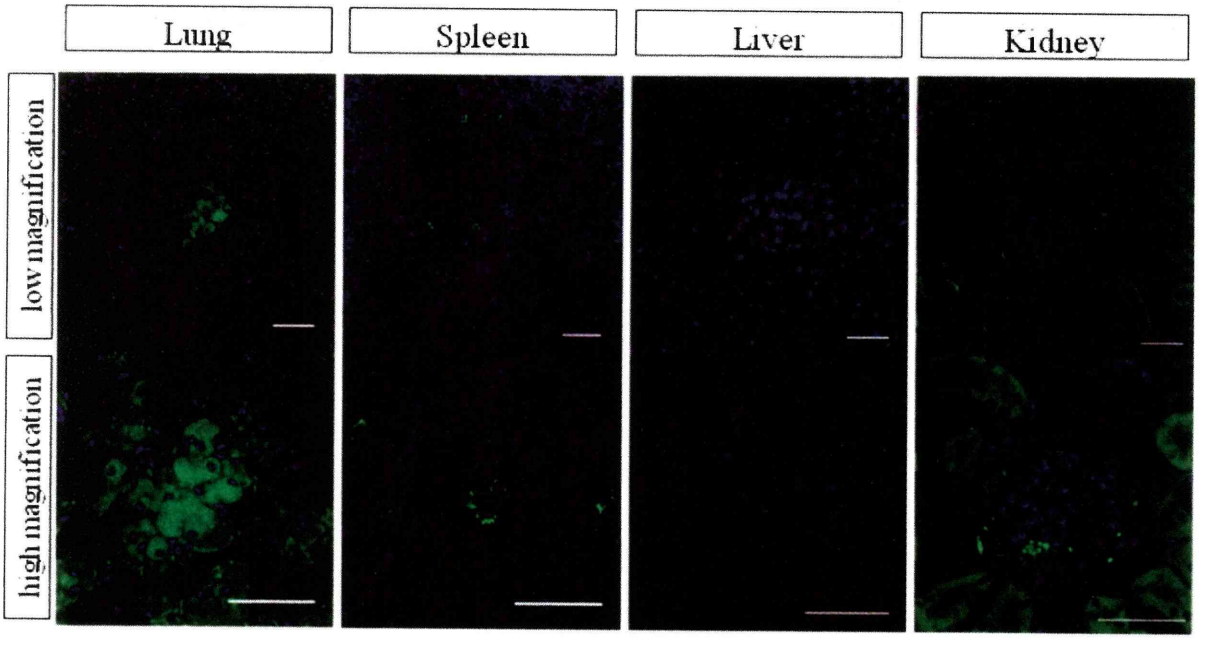

Figure 6. Immunohistochemical analysis of the several organs in the IV group. ffLuc-positive cells were found in the lung and spleen at 6 weeks after transplantation. Many ffLuc-positive fragments were also observed in the kidney, suggesting that degraded grafted cells had been trapped in the glomeruli. Scale bar: 50 μm.

lective ablation of the grafted cells in the host spinal cord causes the deterioration of motor function (19), indicating that the long-term survival of grafted cells in the host spinal cord is very important for functional recovery from SCI.

In the present study, we recognized the functional recovery in the IL group according to the behavioral analysis by BMS score (9) as reported previously (27,44,47), but not in the IT and IV groups (data not shown). However, there remained several possibilities that some mice technically might have received cauda equina impediment by IT injection and that some mice transplanted by femoral vein injection might also have suffered from postoperative scar formation producing hip joint contracture. Thus, further studies would be necessary to obtain a conclusive result in terms of functional recovery. The timing of cell transplantation is critical for the survival of grafted cells because microenvironments of injured spinal cord such as neurotrophic factors, proinflammatory cytokines, chemokines, and free radicals are different among the acute, subacute, and chronic phases of SCI (23,41,49,58). Previous studies indicated that the intralesionally grafted cells at the subacute phase showed better survival than at the acute phase (51). In the present study, we dared to choose the acute phase transplantation because the repair of blood–brain barrier and glial scar formation, which occur at the subacute and chronic phase, could prevent the grafted cells from infiltrating into the injured spinal cord after IT or IV injection at the subacute or chronic phase (57,68).

In the present study, all 10 of the animals in the IV group showed bioluminescence in the chest immediately after transplantation, three died immediately after the injection, and two more died within 4 days, due to pulmonary embolism. To reduce the risk of embolism, the grafted cells should be dissociated completely into single cells, or large cell clusters should be eliminated by filtration. However, complete dissociation of the grafted cells could decrease cell viability compared with the viability of small clusters. Furthermore, because both the IV and IT applications resulted in grafted cells homing to nonlesion sites, longer term observation is needed to evaluate tumor formation.

In conclusion, the transplantation of NS/PCs by IL injection resulted in the best survival of grafted cells among the three methods investigated, and no complications were seen afterwards. Transplantation by IT injection resulted in low survival of the grafted cells at the lesion site, and some cells were detected on the surface of the uninjured spinal cord, along the subarachnoid space. After the IV application, no grafted cells were detected at the SCI site, whereas luminescence was observed in the bilateral chest of all these mice, suggesting that the grafted cells caused pulmonary embolism immediately after the IV injection. Taken together, our findings indicate that the best method for the transplantation of NS/PCs into the SCI site is by IL injection, in terms of both grafted cell survival and safety of the recipient.

ACKNOWLEDGMENTS: We thank T. Harada for expert animal care and S. Miyao for technical support. This work was supported by grants from the Key Technology Project for the Realization of Regenerative Medicine from the Ministry of Education, Culture, Sports, Science and Technology (MEXT) Japan to M.N. and H.O.; the General Insurance Association of Japan to M.N. and Y.T.; and a Grant-in-Aid for the Global COE program from MEXT to Keio University.

REFERENCES

1. Aicher, A.; Brenner, W.; Zuhayra, M.; Badorff, C.; Massoudi, S.; Assmus, B.; Eckey, T.; Henze, E.; Zeiher, A. M.; Dimmeler, S. Assessment of the tissue distribution of transplanted human endothelial progenitor cells by radioactive labeling. Circulation 107(16):2134–2139; 2003.
2. Amariglio, N.; Hirshberg, A.; Scheithauer, B. W.; Cohen, Y.; Loewenthal, R.; Trakhtenbrot, L.; Paz, N.; Koren-Michowitz, M.; Waldman, D.; Leider-Trejo, L.; Toren, A.; Constantini, S.; Rechavi, G. Donor-derived brain tumor following neural stem cell transplantation in an ataxia telangiectasia patient. PLoS Med. 6(2):e1000029; 2009.
3. Arbab, A. S.; Yocum, G. T.; Kalish, H.; Jordan, E. K.; Anderson, S. A.; Khakoo, A. Y.; Read, E. J.; Frank, J. A. Efficient magnetic cell labeling with protamine sulfate complexed to ferumoxides for cellular MRI. Blood 104(4):1217–1223; 2004.
4. Bai, H.; Suzuki, Y.; Noda, T.; Wu, S.; Kataoka, K.; Kitada, M.; Ohta, M.; Chou, H.; Ide, C. Dissemination and proliferation of neural stem cells on the spinal cord by injection into the fourth ventricle of the rat: A method for cell transplantation. J. Neurosci. Methods 124(2):181–187; 2003.
5. Bakshi, A.; Barshinger, A. L.; Swanger, S. A.; Madhavani, V.; Shumsky, J. S.; Neuhuber, B.; Fischer, I. Lumbar puncture delivery of bone marrow stromal cells in spinal cord contusion: A novel method for minimally invasive cell transplantation. J. Neurotrauma 23(1):55–65; 2006.
6. Bakshi, A.; Hunter, C.; Swanger, S.; Lepore, A.; Fischer, I. Minimally invasive delivery of stem cells for spinal cord injury: Advantages of the lumbar puncture technique. J. Neurosurg. Spine 1(3):330–337; 2004.
7. Ban, D. X.; Kong, X. H.; Feng, S. Q.; Ning, G. Z.; Chen, J. T.; Guo, S. F. Intraspinal cord graft of autologous activated Schwann cells efficiently promotes axonal regeneration and functional recovery after rat's spinal cord injury. Brain Res. 1256:149–161; 2009.
8. Barnabe-Heider, F.; Frisen, J. Stem cells for spinal cord repair. Cell Stem Cell 3(1):16–24; 2008.
9. Basso, D. M.; Fisher, L. C.; Anderson, A. J.; Jakeman, L. B.; McTigue, D. M.; Popovich, P. G. Basso mouse scale for locomotion detects differences in recovery after spinal cord injury in five common mouse strains. J. Neurotrauma 23(5):635–659; 2006.
10. Bottai, D.; Madaschi, L.; Di Giulio, A. M.; Gorio, A. Viability-dependent promoting action of adult neural precursors in spinal cord injury. Mol. Med. 14(9–10):634–644; 2008.
11. Brenner, W.; Aicher, A.; Eckey, T.; Massoudi, S.; Zuhayra, M.; Koehl, U.; Heeschen, C.; Kampen, W. U.;